THIN-WIRE RECIPROCAL MULTIRADIUS IMPLEMENTATION OF THE ELECTROMAGNETIC MOMENT METHOD

by

Mark A. Tilston

A thesis submitted in conformity with the requirements

for the Degree of Doctor of Philosophy in the

University of Toronto

Department of Electrical Engineering

University of Toronto

Toronto, Ontario

© Mark A. Tilston

1989

ABSTRACT

The original version of the *uniradius* thin-wire frequency-domain moment-method program developed by J.H. Richmond has been re-formulated to suppress the computation of non-physical asymmetric fields. Two alternative new versions are described, termed the point-charge version and the bridge-current version. The original program and the two new versions are compared with each other and with simplified theory, where applicable, on the following symmetrical structures: a rectangular wire loop, a two-wire transmission line, a coaxial-cage transmission line, and a log-periodic dipole antenna. The bridge-current version is shown to be the most accurate, and the most invariant with respect to variations in segmentation for the above structures. It is noted that this version is particularly advantageous for structures that include close-spaced parallel wires connected by short wire segments.

An implementation of the moment method for electromagnetic analysis of *multiradius* thin-wire structures, including multiwire, multiradius junctions is presented. It is an extension of the uniradius bridge-current re-formulation of J.H. Richmond's uniradius thin-wire theory described above. The method features an exactly symmetric mutual impedance matrix ensuring reciprocity between sources, it is unconstrained with respect to both the length ratio and the radius ratio of adjoining segments, and it permits the self-consistent inclusion of coaxial-cable sections in the configuration under analysis. The method is validated (a) through comparison with simplified theory and an alternative moment-method analysis on both an electrically small rectangular loop and a short coaxial cage transmission line, (b) through comparison with transmission-line theory for a two-wire line and a coaxial cable, (c) through comparison with measurements on a folded

monopole antenna, a sleeve monopole antenna, and a log-periodic dipole antenna, and (d) through comparison with the uniradius bridge-current moment method and transmission-line theory for a bazooka-balun-fed dipole antenna.

Comparison is made between the presented moment method, the NEC (version #1) moment method, and the MININEC moment method, on the analysis of a detuning stub used to minimize the reradiation of AM broadcast signals from a grounded tower, and on the analysis of a bent two-wire transmission line whose dimensions are typical of what one would find on a printed circuit board. In these two specific problems, the presented moment method is shown to be a significant improvement over the NEC and MININEC moment methods.

ACKNOWLEDGEMENTS

The research reported in this thesis was sponsored by Bell Canada, by the Natural Sciences and Engineering Research Council of Canada under Operating Grant A-4140, and by the Ontario Information Technology Research Centre.

The author wishes to acknowledge with gratitude the assistance provided by Professor Keith G. Balmain, through his expert guidance and keen interest, and by the author's late father Dr. William V. Tilston, through his many enthusiastic discussions on antennas and electromagnetic theory.

TABLE OF CONTENTS

1. INTRODUCTION 1

2. ON THE SUPPRESSION OF ASYMMETRIC ARTIFACTS IN THE METHOD OF MOMENTS 7

- 2.1. Introduction 7
- 2.2. Richmond's Original Program 8
- 2.3. Point-Charge Version 12
- 2.4. Bridge-Current Version 15
- 2.5. Comparative Results of the Program Versions 19
  - 2.5.1. Rectangular Loop 19
  - 2.5.2. Resonant Two-Wire Stub 22
  - 2.5.3. Nonresonant Open-Circuited Transmission Line 24
  - 2.5.4. Resonant Open-Circuited Transmission Line 26
  - 2.5.5. Short-Circuited Coaxial Cage Transmission Line 26
  - 2.5.6. Log-Periodic Dipole Antenna 32
- 2.6. Conclusions 33

3. A MULTIRADIUS RECIPROCAL IMPLEMENTATION OF THE THIN-WIRE MOMENT METHOD 35

- 3.1. Introduction 35
- 3.2. Description of the Moment-Method Versions 35
  - 3.2.1. Uniradius Bridge-Current Version 35
  - 3.2.2. Multiradius Bridge-Current Version 37
  - 3.2.3. Transmission-Line Multiradius Version 39
- 3.3. Validation of the Multiradius Moment-Method Version 42
  - 3.3.1. Rectangular Loop 43
  - 3.3.2. Short-Circuited Coaxial Cage Transmission Line 47
  - 3.3.3. Resonant Two-Wire Quarter-Wave Stub 47
  - 3.3.4. Folded Monopole Antenna 51
  - 3.3.5. Sleeve Monopole Antenna 53
  - 3.3.6. Log-Periodic Dipole Antenna 60
  - 3.3.7. Coaxial Cable Stub 63
  - 3.3.8. Bazooka Balun Feed for a Dipole Antenna 65
- 3.4. Conclusions 69

4. ADVANTAGES OF THE BRIDGE-CURRENT MOMENT METHOD OVER OTHER THIN-WIRE MOMENT METHODS 72

4.1. Introduction 72
4.2. Tower Detuning Stub 73
4.3. Bent Two-Wire Transmission Line 76
4.4. Conclusions 78

5. CONCLUSIONS 79

APPENDICES

A INTEGRATION OF THE INTEGRAL I_{pq} 80

B MAGNETIC RING SOURCE AND FRILL SOURCE EXCITATION 85

REFERENCES 90

1. INTRODUCTION

This section introduces some basic terminology, including a brief description of the moment method.

The method of electromagnetic analysis employed is an equivalent surface-current approach whereby the original *physical* problem involving a medium with metallic conductors (case "p") is replaced by one in which *equivalent* electric and magnetic surface currents flow in a completely homogeneous medium (case "e").

The above situation is depicted in Figure 1-1. Case "p" is the physical problem in which $\mathbf{J}_g$ and $\mathbf{M}_g$ are impressed sources (generators) of electric and magnetic current, $\mathbf{E}_p$ and $\mathbf{H}_p$ are the resultant field strengths. The permittivity ε_1 of the conductor is complex, and includes the conductivity of the metal.

Case "e" is an equivalent problem in which $\mathbf{J}_e^s$ and $\mathbf{M}_e^s$ are equivalent electric and magnetic surface currents. They are defined by the condition that the field strength outside S is the same as in case "p", while the field strength inside S is zero. This requires that

$$\mathbf{J}_e^s = \hat{\mathbf{n}} \times \mathbf{H}_p \,, \tag{1-1}$$

$$\mathbf{M}_e^s = \mathbf{E}_p \times \hat{\mathbf{n}} \tag{1-2}$$

where $\hat{\mathbf{n}}$ is the outward normal of S.

In case "e", the medium inside S has been replaced with the external medium. This does not disturb the field anywhere because of the zero field inside S.

Case "p" (physical problem):

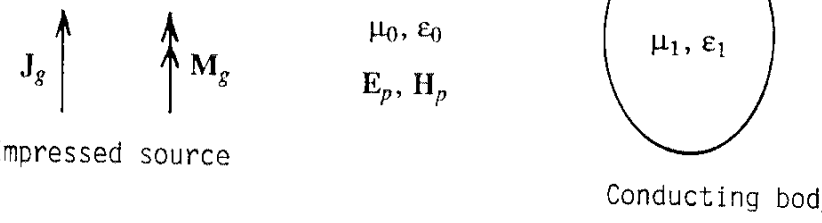

Case "e" (exterior equivalence):

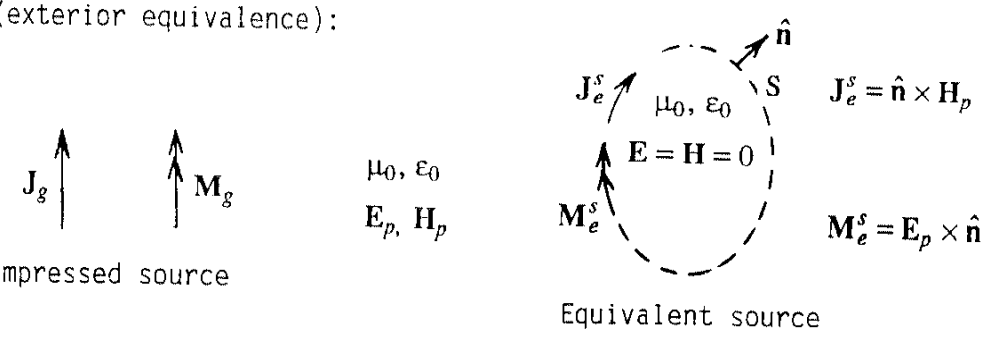

Case "t" (testing source):

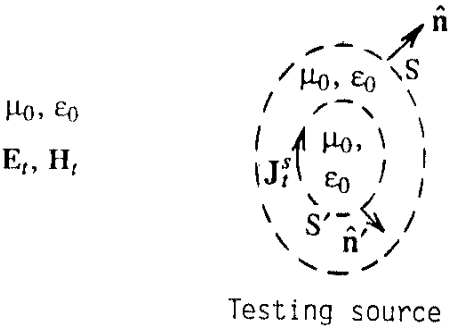

Fig. 1-1 Cases to which the equivalence principle and the reciprocity principle are applied. Cases shown are the physical problem, an exterior equivalence, and a testing source arrangement.

Consider a third case, case "t" in which the medium is the same as in case "e", and an electric surface current $\mathbf{J}_t^s$ flows on a surface S' inside S. Applying the reciprocity principle to cases "e" and "t",

$$\int_V (\mathbf{E}_t \cdot \mathbf{J}_g - \mathbf{H}_t \cdot \mathbf{M}_g)\, dV + \int_S (\mathbf{E}_t \cdot \mathbf{J}_e^s - \mathbf{H}_t \cdot \mathbf{M}_e^s)\, dS$$
$$= \int_{S'} (\mathbf{E}_e + \mathbf{E}_g) \cdot \mathbf{J}_t^s\, dS' \tag{1-3}$$

The right-hand side of the above equation is zero because the total field strength of the equivalent sources plus the impressed sources is zero inside S, where $\mathbf{J}_t^s$ is located. Equating the left-hand side of (1-3) to zero yields

$$-\int_S (\mathbf{E}_t \cdot \mathbf{J}_e^s - \mathbf{H}_t \cdot \mathbf{M}_e^s)\, dS = \int_V (\mathbf{E}_t \cdot \mathbf{J}_g - \mathbf{H}_t \cdot \mathbf{M}_g)\, dV \tag{1-4}$$

This is an integral equation in which only $\mathbf{J}_e^s$ and $\mathbf{M}_e^s$ are unknowns. In the right-hand side of (1-3), $\mathbf{J}_t^s$ is performing a *test* of the electric field inside S in case "e". For example, if $\mathbf{J}_t^s$ was a vertically oriented current element located at some point inside S, the right-hand side of (1-3) would provide a measure of the vertical component of the total electric field at that point in case "e". For this reason, $\mathbf{J}_t^s$ is called a *testing function.*

To simplify the solution of (1-4), a surface impedance approximation can be made in which the tangential electric field $\mathbf{E}_{\tan}$ on the surface of the conductor is related to the equivalent surface current $\mathbf{J}_e^s$ and the surface impedance Z_s by

$$\mathbf{E}_{\tan} \simeq Z_s\, \mathbf{J}_e^s \tag{1-5}$$

Inserting the above in (1-2),

$$\mathbf{M}_e^s \simeq Z_s \, \mathbf{J}_e^s \times \hat{\mathbf{n}} \tag{1-6}$$

Inserting the above in (1-4),

$$-\int_S (\mathbf{E}_t - Z_s \, \hat{\mathbf{n}} \times \mathbf{H}_t) \cdot \mathbf{J}_e^s \, dS = \int_V (\mathbf{E}_t \cdot \mathbf{J}_g - \mathbf{H}_t \cdot \mathbf{M}_g) \, dV \tag{1-7}$$

In this integral equation, only $\mathbf{J}_e^s$ is unknown.

The moment method solves (1-7) by approximating $\mathbf{J}_e^s$ with N selected current distributions $\mathbf{J}_{ej}^s$, called *expansion functions*,

$$\mathbf{J}_e^s \simeq \sum_{j=1}^{N} \mathbf{J}_{ej}^s \tag{1-8}$$

Each expansion function $\mathbf{J}_{ej}^s$ includes an unknown terminal current I_{ej}. In addition, N current distributions $\mathbf{J}_{ti}^s$ for testing functions are chosen, which include terminal currents I_{ti}. Let $\mathbf{E}_{ti}$ and $\mathbf{H}_{ti}$ be the electric and magnetic field strengths of the i^{th} testing function. Equation (1-7) now becomes the following system of simultaneous linear algebraic equations in which I_{ej} must be found:

$$-\sum_{j=1}^{N} \int_S (\mathbf{E}_{ti} - Z_s \, \hat{\mathbf{n}} \times \mathbf{H}_{ti}) \cdot \mathbf{J}_{ej}^s \, dS$$

$$= \int_V (\mathbf{E}_{ti} \cdot \mathbf{J}_g - \mathbf{H}_{ti} \cdot \mathbf{M}_g) \, dV \ , \qquad i = 1 \ , \ N \tag{1-9}$$

Define matrix elements Z_{ij} , Z'_{ij} and V_i as follows:

$$Z_{ij} = -\frac{1}{I_{ti} I_{ej}} \int_S \mathbf{E}_{ti} \cdot \mathbf{J}_{ej}^s \, dS \ , \tag{1-10}$$

$$Z'_{ij} = \frac{1}{I_{ti} I_{ej}} \int_S Z_s (\hat{\mathbf{n}} \times \mathbf{H}_{ti}) \cdot \mathbf{J}_{ej}^s \, dS \ , \tag{1-11}$$

$$V_i = \frac{1}{I_{ti}} \int_V (\mathbf{E}_{ti} \cdot \mathbf{J}_g - \mathbf{H}_{ti} \cdot \mathbf{M}_g) \, dV \tag{1-12}$$

Inserting (1-10), (1-11) and (1-12) into (1-9) yields

$$\sum_{j=1}^{N} (Z_{ij} + Z'_{ij})\, I_{ej} = V_i \,, \qquad i = 1 \,,\ N \tag{1-13}$$

The above equations are valid for general conducting bodies. Specializing now to thin wires, it is assumed that the equivalent electric current on the wire surface is axially directed and uniformly distributed around the wire. Expansion functions are chosen to be likewise axially directed and uniformly distributed around the wire. In addition, testing functions are chosen to be identical to the expansion functions, with S′ equal to S. This allows the subscripts "t" and "e" to be deleted from (1-10) through (1-13).

In equation 1-11, it will be assumed that for thin wires,

$$\mathbf{J}^s_{ti} = \hat{\mathbf{n}} \times \mathbf{H}^s_{ti} \tag{1-14}$$

and (1-11) becomes

$$Z'_{ij} = \frac{1}{I_{ti} I_{ej}} \int_S Z_s\, \mathbf{J}^s_{ti} \cdot \mathbf{J}^s_{ej}\, dS \tag{1-15}$$

where again, the "t" and "e" subscripts can be dropped.

The specific moment method presented here conceptually uses identical overlapping tubular dipoles of electric surface current, conformal with the metallic surfaces, for both expansion and testing. This concept, however, is implemented only approximately through a filamentary current approximation. As will be shown later, the approximation is good for a wide range of structures.

An alternative to tubular currents for testing is filamentary currents, lying along the wire axis. A detailed mathematical description of this formulation is given by J.H. Richmond [1] for the *uniradius* geometry, that is, the geometry in which all wires have the

same radius. However, the actual uniradius implementations of both formulations use similar filamentary current approximations. On the other hand, in developing a *multiradius* implementation, the two formulations would lead to different filamentary current approximations, and the former formulation is used here.

The filamentary current approximations mentioned above are defined precisely in the sections to follow.

2. ON THE SUPPRESSION OF ASYMMETRIC ARTIFACTS IN THE METHOD OF MOMENTS

2.1. INTRODUCTION

A thin-wire frequency-domain moment-method program was developed by J.H. Richmond [1] to analyze antennas and scattering structures that can be modelled by interconnected wire segments. This program has been found to be useful for a wide variety of problems. For example, the program has been used by Vainberg and Balmain [2] to analyze asymmetry resonances in log-periodic dipole antennas, and by Silva, Balmain and Ford [3] to analyze the reradiation of medium frequency AM broadcast signals by steel-tower power lines.

Despite the program's usefulness, it has the defect that its results can depend on the numbering scheme of segment endpoints. In addition, it can predict asymmetrical currents in a structure whose geometry and excitation are symmetrical. Examples of the renumbering and asymmetry problems will be discussed later for a rectangular wire loop, a two-wire transmission line, a coaxial-cage transmission line, and a log-periodic dipole antenna.

The renumbering and asymmetry problems exist because the program computes only the mutual impedance between expansion and testing functions for elements in the upper right triangular portion (including the main diagonal) of the moment method mutual impedance matrix. It is assumed that the mutual impedance elements are symmetrical. However, as shall be shown later, this assumption can be incorrect under some circumstances, resulting in the problems mentioned above. A solution is to re-formulate the method in order to produce truly symmetrical mutual impedance elements. This

solution has the desirable features of producing reciprocity between ports on the wire structure as there should be in reality, and allowing minimal matrix inversion time and computer storage requirements because of the symmetrical matrix.

2.2. RICHMOND'S ORIGINAL PROGRAM

In the concept behind the original program, the current expansion functions are set up as overlapping tubular dipolar distributions of piecewise-sinusoidal surface current. The current of an expansion dipole is axially directed, has a piecewise-sinusoidal distribution in the axial coordinate, and has no azimuthal variation. Each arm of a dipole (i.e. monopole) spans one wire segment. Each junction of N segments is the vertex of $N-1$ independent dipoles.

In Richmond's formulation, each expansion function has a corresponding testing function that spans the same length of wire, and has the same axial distribution of current, but has a different cross-sectional distribution which is filamentary along the wire axis. Because of the latter difference between an expansion function and its corresponding testing function, the mutual impedance matrix is not precisely symmetric. In other words, the reaction between a tubular expansion dipole "a" and a filamentary testing dipole "b" can differ from the reaction between the corresponding filamentary testing dipole "a" and tubular expansion dipole "b". This asymmetry would occur, for example, in the case of two non-collinear dipoles of different lengths.

In Richmond's implementation of the above formulation, an approximation is made which can lead to an exactly symmetric mutual impedance matrix. The computation of mutual impedance between a tubular expansion dipole and a filamentary testing dipole is

composed of four monopole-to-monopole mutual impedances. In the mutual impedance between an expansion monopole and a testing monopole, the tubular expansion monopole is replaced by an approximately equivalent filamentary expansion monopole. In a filamentary monopole-to-monopole mutual impedance computation, the two monopoles are placed on their respective segment axes unless the axes intersect or coincide. If the axes coincide, the monopoles are offset from each other by a wire radius in a direction orthogonal to the coincident axes. In this coincident-axis case, the equivalence between the tubular and filamentary expansion monopoles is exact because of symmetry. If the two segment axes intersect, the monopoles are offset from each other by a wire radius in a direction orthogonal to the plane containing both axes.

Figure 2-1 illustrates the arrangement of segment axes in an example dipole-to-dipole mutual impedance calculation. Circled letters denote dipoles and boxed numbers denote monopoles. The unenclosed numbers denote points on the wire axes that define the span of two dipoles. Each dipole contains two monopoles. The mutual impedance between dipole "a" and dipole "b" is composed of four monopole-to-monopole mutual impedances as follows:

$$Z_{ab} = Z_{13} + Z_{14} + Z_{23} + Z_{24}$$

$$Z_{ba} = Z_{31} + Z_{32} + Z_{41} + Z_{42}$$

Of the above pairs of monopoles, those requiring an offset are 2-3 and 2-4. Pairs 1-3 and 1-4 do not require an offset because their segment axes do not intersect. Figure 2-2 shows a possible monopole geometry that satisfies the offset requirements for both Z_{ab} and Z_{ba}. The mutual impedance Z_{ab} is computed with the same current distributions as Z_{ba}, so Z_{ab} and Z_{ba} are reciprocal. Note that monopoles 1 and 2 are offset

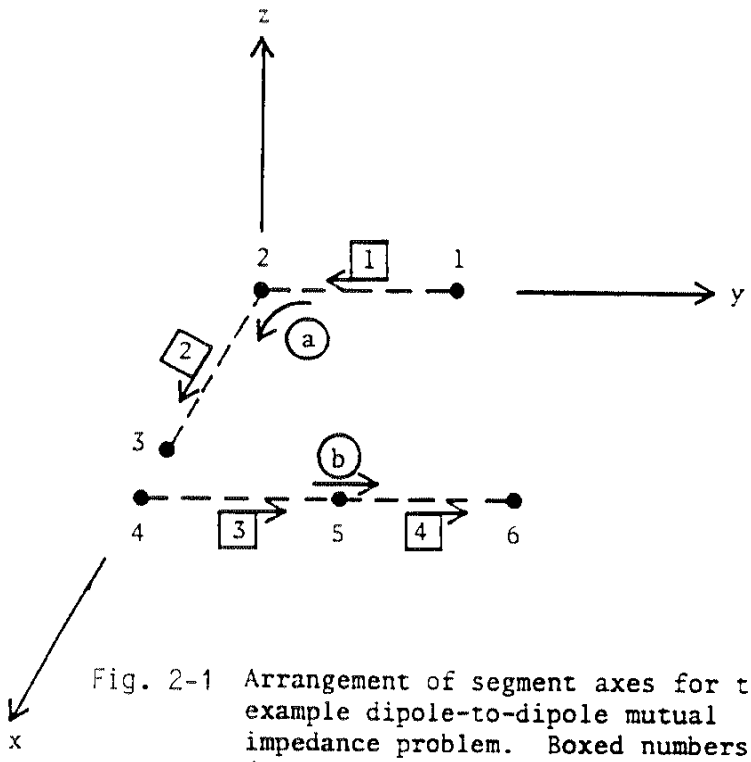

Fig. 2-1 Arrangement of segment axes for the example dipole-to-dipole mutual impedance problem. Boxed numbers denote monopoles, circled letters denote dipoles, unenclosed numbers denote axis point numbers. Arrows indicate reference direction for current flow.

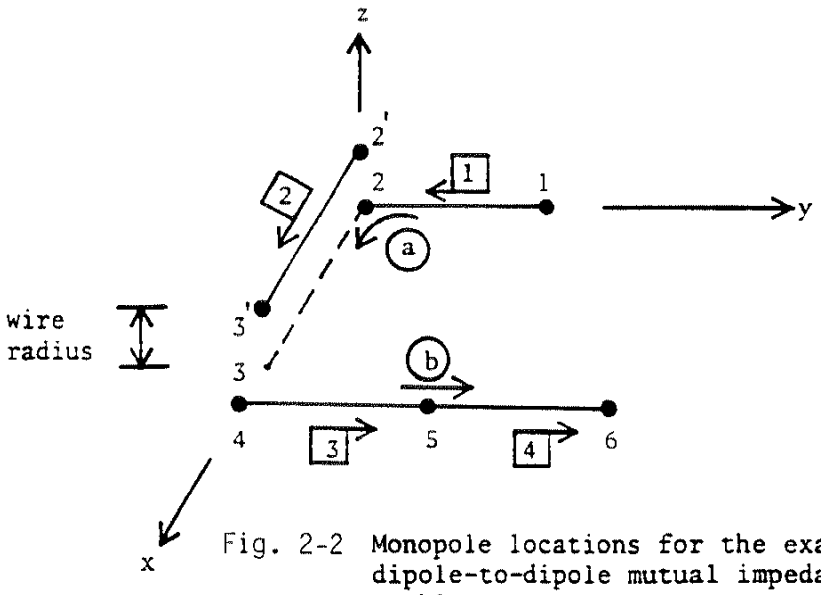

Fig. 2-2 Monopole locations for the example dipole-to-dipole mutual impedance problem.

from one another causing dipole "a" to be broken, while dipole "b" is continuous. To satisfy the continuity equation, there must be equal and opposite point charges on monopoles 1 and 2 at the dipole break. However, in the original program, the contribution of the point charge electric scalar potential gradient is not included in the **E** field when the following mutual impedance integrals are evaluated:

$$Z_{ab} = -(I_a I_b)^{-1} \int \mathbf{E}_a \cdot \mathbf{J}_b \, dV \tag{2-1a}$$

$$Z_{ba} = -(I_a I_b)^{-1} \int \mathbf{E}_b \cdot \mathbf{J}_a \, dV \tag{2-1b}$$

where $\mathbf{E}_a$ and $\mathbf{E}_b$ are the electric fields of dipoles "a" and "b", $\mathbf{J}_a$ and $\mathbf{J}_b$ are the volume current densities of dipoles "a" and "b", I_a and I_b are the dipole terminal currents (unit terminal current is assumed hereafter), and the integrations cover all space. This neglect of the point charges will affect $\mathbf{E}_a$, but not $\mathbf{E}_b$ (because dipole "b" has no point charges). Hence, Z_{ab} will be affected, but not Z_{ba}, and reciprocity cannot hold.

To restore reciprocity to the above situation where one dipole is broken, two alternative re-formulations were implemented. The first involves partial inclusion of the point charge contribution to (2-1a), resulting in the *point-charge version* of the program. The second involves creating a bridging current in the broken dipole to flow across the break, resulting in the *bridge-current version* of the program. These two versions will be discussed in the next sections. Another version that included the full point charge contribution was found to be less accurate, and is not covered here.

As noted earlier in this section, Richmond's formulation, if implemented exactly, would not yield a precisely symmetric mutual impedance matrix. However, the approximate implementation, which involves only filamentary currents, leads to an exactly symmetric matrix, provided that broken dipoles are handled carefully. Because the

approximation is symmetric, the author prefers to view it as representing a formulation that is also symmetric. The preferred symmetric formulation is one in which each tubular expansion function has a corresponding identical tubular testing function.

2.3. POINT-CHARGE VERSION

The point-charge version was developed as an early and successful attempt to eliminate the non-physical asymmetric currents in the computation of asymmetry resonances in log periodic dipole antennas [4].

As mentioned in the previous section, the original program does not include the point charge electric scalar potential contribution to the **E** field when computing the mutual impedance in (2-1a). This neglected point charge contribution is included in the point-charge version, though not in its entirety. It will be shown that the point charge contribution contains a symmetric and an asymmetric component. Only the asymmetric component is included because it is the minimum addition that is required to restore symmetry to the mutual impedance. Consider the mutual impedance between two filamentary monopoles depicted in Figure 2-3 in which monopole "s" lies on the s axis, monopole "t" lies on the t axis, and each monopole has unit terminal current, where the terminals are at points s_1 and t_1. The mutual impedance is

$$Z_{st} = -\int \mathbf{E}_s(t) \cdot \mathbf{I}_t(t)\, dt \tag{2-2}$$

where $\mathbf{E}_s$ is the electric field of monopole "s", and $\mathbf{I}_t$ is the line current of monopole "t". In terms of the electric scalar potentials Φ and Φ' of the distributed charge and the point charge at s_1, and the magnetic vector potential **A**, the **E** field is

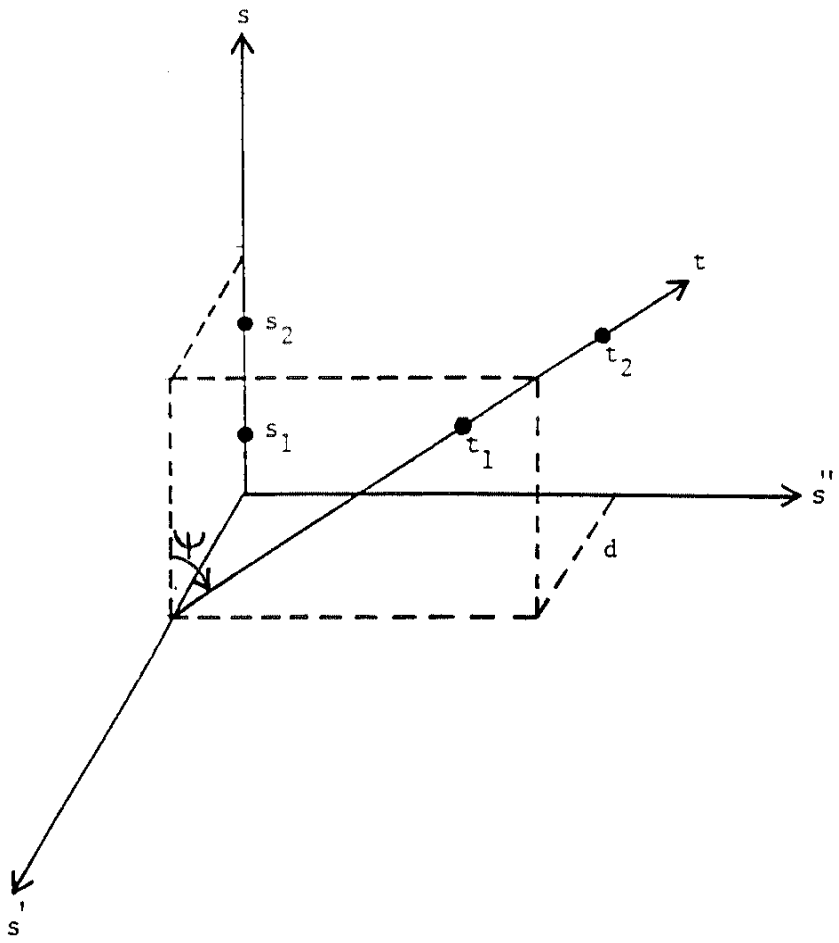

Fig. 2-3 Coordinate system used to analyze the mutual impedance between two monopoles.

$$\mathbf{E}_s(t) = -j\omega \mathbf{A}_s(t) - \nabla \Phi_s(t) - \nabla \Phi_s'(t) \tag{2-3a}$$

$$\Phi_s(t) = \frac{1}{4\pi\varepsilon} \int q_s(s) \frac{e^{-\gamma R(s,t)}}{R(s,t)} ds \quad , \tag{2-3b}$$

$$\Phi_s'(t) = \frac{Q_s}{4\pi\varepsilon} \frac{e^{-\gamma R(s_1,t)}}{R(s_1,t)} \tag{2-3c}$$

$$\mathbf{A}_s(t) = \frac{\mu}{4\pi} \int \mathbf{I}_s(s) \frac{e^{-\gamma R(s,t)}}{R(s,t)} ds \quad , \tag{2-3d}$$

$$R(s,t) = |\mathbf{r}(s) - \mathbf{r}(t)| \quad , \tag{2-3e}$$

and

$$\gamma = j\omega\sqrt{\mu\varepsilon} \tag{2-3f}$$

where q_s is the line charge of monopole "s", and Q_s is the point charge of monopole "s". When (2-3a) is substituted into (2-2), Z_{st} is composed of three terms. The term arising from the point charge contribution is

$$Z_{st}' = \int \nabla \Phi_s'(t) \cdot \mathbf{I}_t(t)\, dt \quad . \tag{2-4}$$

This is the point charge contribution that was neglected in the original program. After integrating (2-4) by parts and applying the continuity equation, the Z_{st}' can be expressed as follows:

$$Z_{st}' = \frac{j\omega Q_s Q_t}{4\pi\varepsilon} \frac{e^{-\gamma R(s_1,t_1)}}{R(s_1,t_1)} + \frac{j\omega Q_s}{4\pi\varepsilon} \int q_t(t) \frac{e^{-\gamma R(s_1,t)}}{R(s_1,t)} dt \tag{2-5}$$

The first term in (2-5) is a point-to-point term. It is symmetrical, i.e. the corresponding term in a Z_{ts}' calculation would be identical. Therefore the addition of this term to the original program cannot restore reciprocity to the mutual impedance between monopoles, hence it was not added. The second term in (2-5) is a point-to-line term: it is asymmetrical, and must compensate for the asymmetry already existing in the original program. Thus for the point-charge version, the point-to-line term of (2-5) was added to the

original program. For the sinusoidal current distribution used in the program, the point-to-line term can be evaluated in terms of the exponential integral.

2.4. BRIDGE-CURRENT VERSION

In section 2.1., it was shown that a broken dipole can arise in the original program. In the bridge-current version, a new current is introduced to bridge any break in a dipole. For example in Figure 2-2, a bridge current would flow from point 2 to $2'$. For simplicity, the bridge current is chosen to be a constant across the break. To facilitate programming, the mutual impedance integral (2-1a) is rearranged into a symmetric form. This is done by first expressing the **E** field in (2-1a) terms of the electric scalar potential and the magnetic vector potential as shown below.

$$Z_{ab} = \int (j\omega \mathbf{A}_a + \nabla \Phi_a) \cdot \mathbf{J}_b \, dV \tag{2-6}$$

The term involving Φ is integrated by parts as follows:

$$\int \nabla \Phi_a \cdot \mathbf{J}_b \, dV = \oint \Phi_a \, \mathbf{J}_b \cdot d\,\mathbf{S} - \int \Phi_a \, \nabla \cdot \mathbf{J}_b \, dV \tag{2-7}$$

Because the integral is over all space, and because $\mathbf{J}_b$ is of finite extent, it follows that $\mathbf{J}_b$ is zero on S and the surface integral vanishes. The continuity equation relates the charge to the current as

$$\nabla \cdot \mathbf{J}_b = -j\omega\rho_b \quad . \tag{2-8}$$

Combining (2-8), (2-7) and (2-6), we have

$$Z_{ab} = j\omega \int (\mathbf{A}_a \cdot \mathbf{J}_b + \Phi_a \, \rho_b) \, dV \tag{2-9}$$

Substituting for $\mathbf{A}$ and Φ from (2-3) into the above expression yields

$$Z_{ab} = j\omega \int\int \left[\frac{\mu}{4\pi} \mathbf{J}_a(\mathbf{r}') \cdot \mathbf{J}_b(\mathbf{r}) + \frac{1}{4\pi\varepsilon} \rho_a(\mathbf{r}') \rho_b(\mathbf{r}) \right] \cdot \frac{e^{-\gamma R}}{R} dV\, dV' \qquad (2\text{-}10a)$$

where

$$R = | \mathbf{r} - \mathbf{r}' | \quad . \qquad (2\text{-}10b)$$

From (2-10a) it is clear that Z_{ab} and Z_{ba} are equal. In (2-10a) , it is noted that, for short separations, the first term is related to inductive coupling and the second term is related to capacitive coupling.

Consider the application of (2-10a) to the dipoles shown in Figure 2-2, with an added bridge current bridging the break in dipole "a". Because the bridge current is orthogonal to dipole "b", the dot product of the bridge-current part of $\mathbf{J}_a$ and $\mathbf{J}_b$ is zero, and the bridge current does not contribute to the first term of (2-10a). Because the distribution of the bridge current is constant, it has no associated distributed charge, and continuity of current guarantees no end charges, so the bridge current does not contribute to the second term of (2-10a). Hence the bridge current makes no contribution to (2-10a), and can thus be ignored when computing Z_{ab}. Note that the same mutual impedance Z_{ab} would be obtained using (2-1a), although the bridge current would have to be included in the computation.

Because the bridge current can be ignored when using (2-10a), the only change required to the original program is to evaluate the mutual impedance between monopoles using (2-10a) instead of (2-1a), using only the *distributed* charge on the monopoles.

The specific equations will now be described utilizing Richmond's terminology where possible. Figure 2-3 shows two filamentary monopoles of which monopole "s" spans points s_1 and s_2, and monopole "t" spans points t_1 and t_2. The current dis-

tributions are as follows:

On monopole "s",

$$\mathbf{I}_i(s) = \hat{s}\,\frac{\sinh\gamma(s - s_k)}{\sinh\gamma(s_i - s_k)} \tag{2-11}$$

where $i = 1$ or 2, $k = 2/i$ and $s_1 \le s \le s_2$.

On monopole "t",

$$\mathbf{I}_j(t) = \hat{t}\,\frac{\sinh\gamma(t - t_l)}{\sinh\gamma(t_j - t_l)} \tag{2-12}$$

where $j = 1$ or 2, $l = 2/j$ and $t_1 \le t \le t_2$. Utilizing (2-10a), the mutual impedance between monopoles "s" and "t" is:

$$Z_{st}^{ij} = j\omega \int_{t_1}^{t_2} \int_{s_1}^{s_2} \left[\frac{\mu}{4\pi} I_i(s)\, I_j(t) \cos\psi + \frac{1}{4\pi\varepsilon} q_i(s)\, q_j(t)\right] \frac{e^{-\gamma R}}{R}\, ds\, dt \tag{2-13}$$

where $R = \left[s^2 + t^2 - 2st\cos\psi + d^2\right]^{1/2}$ and $d > 0$.

Applying the continuity equation to (2-11) and (2-12) gives q_i and q_j. Substituting the current and charge distributions into (2-13) yields

$$Z_{st}^{ij} = C'_{ij} \int_{t_1}^{t_2} \int_{s_1}^{s_2} \Big[\sinh\gamma(s - s_k)\sinh\gamma(t - t_l)\cos\psi + \cosh\gamma(s - s_k)\cosh\gamma(t - t_l)\Big] \frac{e^{-\gamma R}}{R}\, ds\, dt \tag{2-14}$$

where $C'_{ij} = \dfrac{j\omega\mu}{4\pi \sinh\gamma(s_i - s_k)\sinh\gamma(t_j - t_l)}$.

Expanding the sinh and cosh functions in terms of exponential functions yields

$$Z_{st}^{ij} = C_{ij} \sum_{p=1}^{2} \sum_{q=1}^{2} e^{-\gamma (ms_k + nt_l)} \; mn \, I_{pq} \tag{2-15a}$$

where

$$C_{ij} = \frac{\eta}{16\pi \sinh \gamma (s_i - s_k) \sinh \gamma (t_j - t_l)} \quad , \tag{2-15b}$$

$$\eta = \sqrt{\mu / \varepsilon} \quad , \quad m = (-1)^{p-1} \quad , \quad n = (-1)^{q-1} \quad , \tag{2-15c}$$

and

$$I_{pq} = \gamma \frac{1 + mn \cos \psi}{mn} \int_{t_1}^{t_2} \int_{s_1}^{s_2} \frac{e^{\gamma (ms + nt - R)}}{R} \, ds \, dt \quad . \tag{2-15d}$$

The integral I_{pq} is evaluated in Appendix A. The result is repeated here but with the format changed to facilitate programming.

$$\begin{aligned} I_{pq} = \sum_{h=1}^{2} (-1)^h \Bigg[& - e^{\gamma t_h (n + m \cos \psi)} \int_{v(s_1, t_h)}^{v(s_2, t_h)} \frac{e^{-z}}{z} \, dz \\ & - e^{\gamma s_h (m + n \cos \psi)} \int_{w(s_h, t_1)}^{w(s_h, t_2)} \frac{e^{-z}}{z} \, dz + e^{\gamma j u_0} \int_{x(s_h, t_1)}^{x(s_h, t_2)} \frac{e^{-z}}{z} \, dz \\ & + e^{-\gamma j u_0} \int_{y(s_h, t_1)}^{y(s_h, t_2)} \frac{e^{-z}}{z} \, dz \Bigg] \end{aligned} \tag{2-16}$$

where

$$v(s,t) = \gamma (-ms + mt \cos \psi + R) \quad ,$$

$$w(s,t) = \gamma (-nt + ns \cos \psi + R) \quad ,$$

$$x(s,t) = \gamma (-ms - nt + R + j u_0) \quad ,$$

$$y(s,t) = \gamma (-ms - nt + R - j u_0) \quad ,$$

$$\text{and} \quad u_0 = d \left[\frac{1 + mn \cos \psi}{1 - mn \cos \psi} \right]^{1/2} \quad .$$

Note that each integration variable is a complex constant multiplied by a real function which is sometimes added to an imaginary constant. The integration path is therefore a

straight line on the complex plane. The function

$$w_{12}(z_1, z_2) = \int_{z_1}^{z_2} \frac{e^{-z}}{z}\, dz \tag{2-17}$$

for a straight line path is evaluated in the original program.

Limiting cases occur when the monopoles are parallel, causing u_0 to be zero or infinite. u_0 becomes zero when $1 + mn \cos\psi$ is zero. In this case, as shown in Appendix A, $I_{pq} = 0$. u_0 becomes infinite when $1 - mn \cos\psi$ is zero. In this case, as shown in the Appendix, the last two terms of I_{pq} in (2-16) vanish.

2.5. COMPARATIVE RESULTS OF THE PROGRAM VERSIONS

Computations using the original program, the point-charge version, and the bridge-current version have been compared with one another for a rectangular wire loop, a two-wire transmission line, a coaxial-cage transmission line, and a log-periodic dipole antenna. For the rectangular loop and the transmission lines, the computations were also compared with simplified theory. The computations were done on a microcomputer having an 8088 microprocessor (8 bit) with an 8087 math coprocessor, using standard Fortran 77. For complex numbers and functions, single precision (i.e. COMPLEX*8) was used except where otherwise noted.

2.5.1. Rectangular Loop

The versions were used to compute the input impedance of a rectangular loop of perfectly conducting wire whose dimensions were 30 mm by 7.5 mm. The wire had a radius of 1.25 mm and had infinite conductivity. The frequency was 100 MHz. Note that

the wire on the short side has a length-to-radius ratio of only 6, whereas a ratio of 10 or more is often preferred to avoid numerical errors. Because this loop is electrically small, i.e. only 0.025λ in perimeter, the input reactance can be computed approximately using an inductance formula. Such a formula is given by the U.S. National Bureau of Standards [5], as follows:

$$L = \frac{\mu}{\pi}\left[(l_1 + l_2)\ln\frac{2l_1\,l_2}{a} - l_1\ln(l_1 + l_d)\right. \tag{2-18}$$

$$\left. - l_2\ln(l_2 + l_d) + 2\,(l_d + a - l_1 - l_2)\right]$$

where the formula has been converted for units of m, H and natural logarithms; l_1, l_2 and l_d are the length, width and diagonal dimensions of the rectangle, and a is the wire radius. Using this formula, the loop inductance is 0.02377 μH, which has a reactance of 14.94 Ω at 100 MHz.

The radiation resistance was computed by means of numerical integration of the radiated power flowing through a spherical surface in the far-field region. A resistance of 19.52 μΩ was obtained.

Figure 2-4 shows various segmentations and corresponding impedances computed with the original program (R), the uniradius point-charge version (UPC), and the uniradius bridge-current version (UBC). For complex numbers and functions, double precision was required to obtain accurate resistances. It can be seen that the bridge-current version is very stable, consistently yielding a resistance in the range of 19.36 to 19.39 μΩ, and yielding a reactance of 14.95 or 14.96 Ω. These results are very close to the impedance of $19.52 \times 10^{-6} + j14.94\Omega$ obtained from the simplified theory. Comparing Figures 2-4(b) and 2-4(c), one sees that the original program predicts reactances that

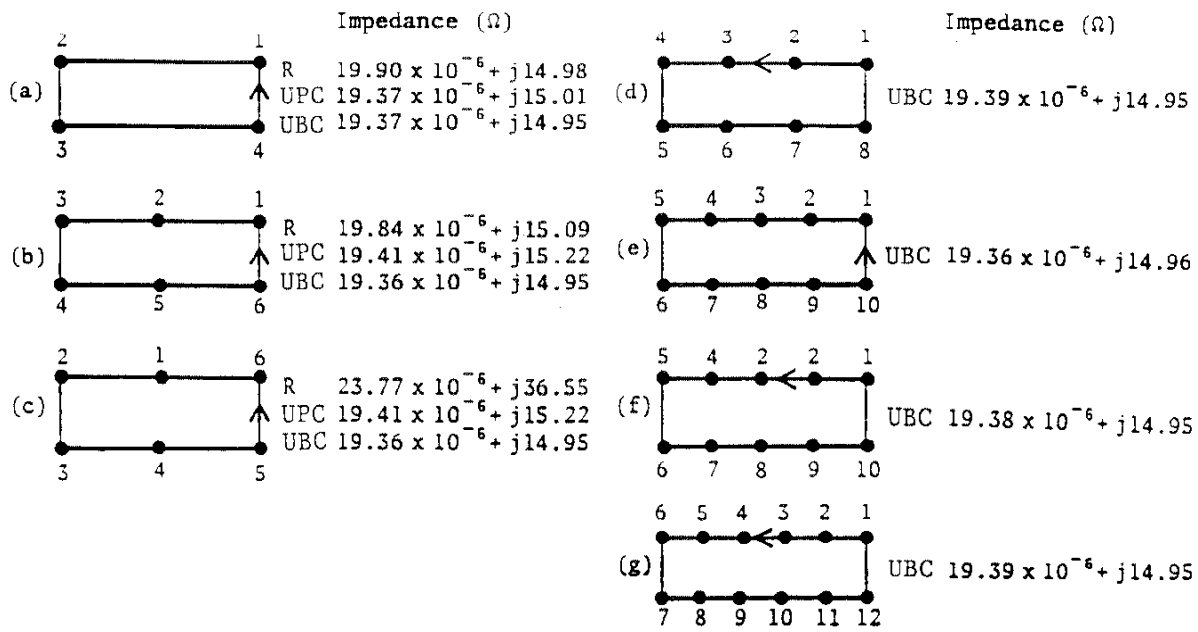

Fig. 2-4 Impedance of a perfectly conducting rectangular wire loop computed by the original Richmond program (R), the point-charge version (UPC), and the bridge-current version (UBC). All computations used double-precision complex numbers and functions. Dots denote segment end points, and arrows denote voltage generators. Voltage generators are located at the segment end at which the arrow points. The impedance obtained from simplified theory is $19.52 \times 10^{-6} + j14.94\ \Omega$.

change from 15.09 to 36.55 Ω , and resistances that change from 19.84 to 23.77 μΩ, solely because the point numbering scheme was changed. In the same two figures, it is seen that the point-charge version does not depend on the point numbering scheme. However, the predictions with this version do change somewhat with segmentation as seen in Figures 2-4(a) and 2-4(b).

In this example of the rectangular loop, the bridge-current version is clearly the most accurate and the most stable.

2.5.2. Resonant Two-Wire Stub

The input reactance was computed, using transmission line theory and the moment method, for the two-wire transmission line stub shown in Figure 2-5(a). The line has a width of 7.5 mm and a length of 750 mm which is 0.25017 λ at the test frequency of 100 MHz. The transmission line is short circuited at one end, and open circuited at the other. The radius of the wire for both the transmission line and the short-circuit is 1.25 mm, and the conductivity is infinite. As with the rectangular loop example, the short-circuiting wire has a length-to-radius ratio of only 6.

Figure 2-5(b) shows the equivalent transmission line circuit. The characteristic impedance Z_0 of a two wire transmission line is

$$Z_0 = 120 \cosh^{-1} \frac{b}{2a} \tag{2-19}$$

where a and b are the wire radius and spacing in m. For this example the characteristic impedance is 211.53 Ω. The propagation constant of the line equals that of free space. The self inductance, L_s, of the short-circuiting wire is approximately the same as the mutual inductance of two parallel filamentary currents spaced a wire radius apart, as

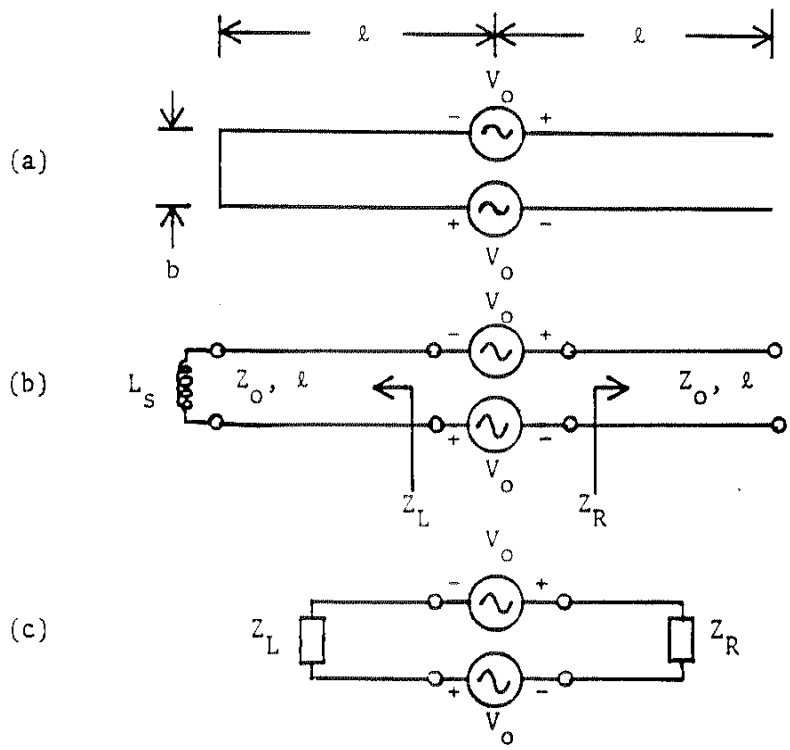

Fig. 2-5 Resonant quarter-wave stub:
(a) dimensions and feed details;
(b) equivalent transmission-line circuit;
(c) equivalent lumped-element circuit.

shown below.

$$L_s = \frac{\mu}{4\pi} \int_0^b \int_0^b \frac{ds\, dt}{\sqrt{(s-t)^2 + a^2}} \tag{2-20a}$$

$$= \frac{\mu b}{2\pi} \left[\sinh^{-1} \frac{b}{a} + \frac{a}{b} - \sqrt{1 + (\frac{a}{b})^2} \right] \tag{2-20b}$$

For this example, the self inductance of the short-circuiting wire is 2.4669×10^{-9} H, which yields a reactance of 1.55 Ω at 100 MHz. The resulting transmission line theory input reactance as defined in Figure 2-5(c) is 3.57 Ω.

Figure 2-6 shows the moment method predicted reactances for various segmentations. The original program (R) is seen to predict reactances that vary with the numbering scheme of the segment end points. However, for any segmentation, there is one numbering scheme that produces predicted reactances that agree well with transmission line theory. The point-charge (UPC) and bridge-current (UBC) versions are insensitive to the point numbering scheme. The slight dependence on numbering is probably due to computer round-off error. The point-charge and bridge-current versions are also insensitive to the number of segments chosen.

In this example, the bridge-current version is slightly more stable and in better agreement with transmission line theory than the point-charge version. Both versions are clearly more stable and more accurate than the original program.

2.5.3. Nonresonant Open-Circuited Transmission Line

The previous example was repeated, but with the short-circuiting wire removed. The resulting input reactance predicted from transmission line theory was $-422.6\ \Omega$.

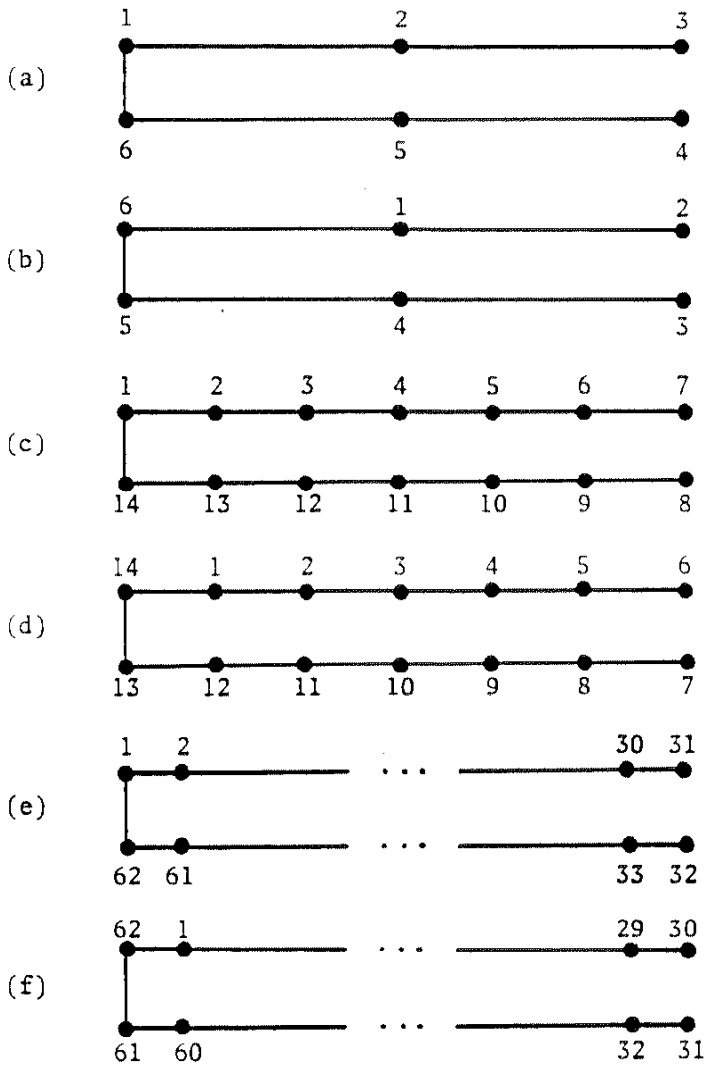

Fig. 2-6 Reactance of quarter wave stub at 100 MHz computed by R, UPC and UBC moment methods. Dots denote segment end points. The stub dimensions and feed details are shown in Figure 2-5 where $\ell = 375$ mm, $b = 7.5$ mm and $a = 1.25$ mm. The wire is assumed to be perfectly conducting. The reactance obtained from transmission-line theory is 3.57 ohms.

Moment method predictions of the input reactance yielded $-423.0\ \Omega$ for all three versions for the segmentations and point numbering schemes tested. Two different segmentations were tested. The first had two segments per wire, and the second had six segments per wire. The reason that the predictions with the original program were independent of point numbering scheme is that no broken dipoles could have been formed.

2.5.4. Resonant Open-Circuited Transmission Line

The previous example was repeated, but with the wire length increased from 0.75 m to 1.50 m. The resulting input reactance computed from transmission line theory was $0.44\ \Omega$.

Moment method predictions of the input reactance yielded $2.02\ \Omega$ with all three versions for two segments per wire, and $2.03\ \Omega$ with all three versions for six segments per wire. As in the previous example, all three versions are independent of the point numbering scheme, and are insensitive to segmentation. However, in this example, the agreement between the moment method and transmission line theory is not quite as good as with the previous examples, the difference between the predicted reactances with the moment method and with transmission line theory being $1.6\ \Omega$.

2.5.5. Short-Circuited Coaxial Cage Transmission Line

The previous transmission-line structures for which the moment method was compared with a simplified theory were planar. In this section, such a comparison is made for a three-dimensional structure, namely, a short-circuited coaxial-cage transmission line. This is similar to a coaxial cable, short-circuited at both ends, but with the outer shield replaced by four wires forming a symmetrical cage around the inner conductor.

Figure 2-7(a) shows the geometry. The rectangular loop formed by any one of the cage wires, the inner wire, and the shorting end-wires, is identical to the rectangular loop discussed previously. In the moment method analyses, the feed point is on one end of the axial wire. In the simplified theory, the feed point is also on the inner wire, but its position on the inner wire does not matter because of the assumed existence of a uniform current.

In the simplified analysis, the current on any wire is approximated by an axially directed current whose axial distribution is uniform. This uniform-current approximation is reasonable because the cage length is only 0.01 wavelengths. The current on each of the four cage wires is one quarter of the current on the inner wire because of symmetry.

To obtain the contribution to the input impedance, of the finite conductivity of the metal, it is assumed that the internal impedance per unit length of the wire, Z_{int}, is the same as for an infinite wire carrying an axially directed current that has no azimuthal variation. The expression for Z_{int} as derived in Jordan and Balmain [6] is

$$Z_{int} = \frac{\eta_m}{2\pi a} \frac{I_0 (\gamma_m a)}{I_1 (\gamma_m a)} \tag{2-21}$$

where η_m and γ_m are the intrinsic impedance and the propagation constant of the metal, a is the radius of the wire, and I_0 and I_1 are modified Bessel functions of the first kind. For the dimensions of Figure 2-7, a conductivity of 57 MS/m, and a frequency of 100 MHz, equation (2-21) yields a value for Z_{int} of 0.3351 + j0.3351 ohms per metre, and the resultant impedance seen at the feed point is 0.01382 + j0.01382 ohms.

The radiation resistance was computed by means of numerical integration of the radiated power flowing through a spherical surface in the far-field region. A resistance of

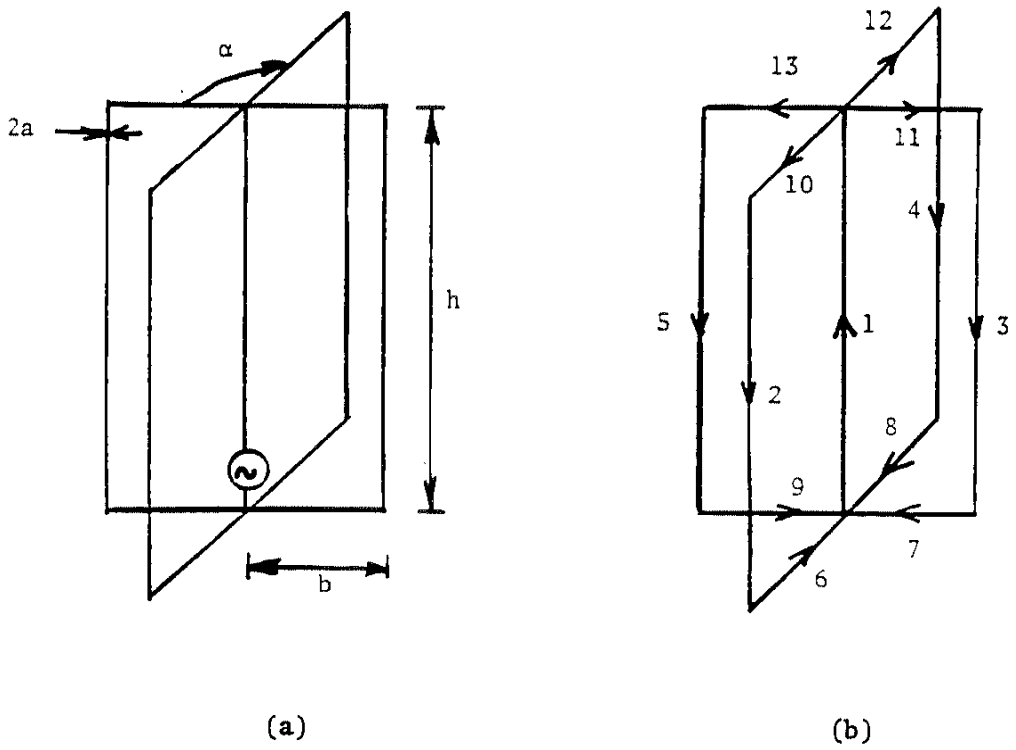

Fig. 2-7 Short-circuited cage transmission line. (a) Geometry in which b = 7.5 mm, h = 30 mm, a = 1.25 mm, and $\alpha = 90°$. (b) Segmentation for magnetostatic analysis. Segment numbers are shown along with arrows to define reference directions for current flow.

3.014×10^{-10} ohms was obtained.

To obtain the contribution of magnetostatic inductance to the input impedance, consider the following formula from Jordan and Balmain [7] for the inductance of a closed circuit containing only one loop:

$$L = \oint \oint \frac{\mu}{4\pi R} d\mathbf{s}' \cdot d\mathbf{s} \tag{2-22}$$

The extension of (2-22) to allow for a closed circuit of multiple loops is

$$L = \int \int \frac{\mu}{4\pi R} I(s') I(s) \, d\mathbf{s}' \cdot d\mathbf{s} \tag{2-23}$$

where the reference direction for current is in the positive s direction, and the current at the feed point is unity. This equation can be arrived at by utilizing (2-10a) along with the approximations that no charge exists, and that the dimensions are so small that the exponential factor in (2-10a) equals unity. If the closed circuit consists of N straight wire segments, each having uniform current, then the inductance L is a sum of segment-to-segment mutual inductances L_{ij} as shown below.

$$L = \sum_{i=1}^{N} \sum_{j=1}^{N} I_i \, I_j \, L_{ij} \tag{2-24a}$$

$$\text{where } L_{ij} = \frac{\mu}{4\pi} \hat{s}_i \cdot \hat{s}_j \int \int \frac{1}{R} ds_i \, ds_j \tag{2-24b}$$

In the cage structure under consideration, segments are either parallel or perpendicular. Perpendicular segments have no mutual inductance according to (2-24b). The mutual inductance between two parallel segments is approximated by the mutual impedance between two filaments of current. If the segments have coincident axes, then the filaments are offset by a wire radius. If the axes are not coincident then the filaments lie

on the axes of their corresponding segments. To evaluate the mutual inductance between two parallel filaments of current, consider the geometry in Figure 2-3, in which $\cos\psi$ is ± 1, and the reference direction for the "s" and "t" currents is in the positive s and t directions. In this case, the mutual inductance evaluated using (2-24b) is

$$L_{st} = \frac{\mu}{4\pi}\left[\left[(t-ms)\ln(ms-t+R)+R\right]_{s_1}^{s_2}\right]_{t_1}^{t_2} \tag{2-25}$$

where $R = \sqrt{(t-ms)^2 + d^2}$ and $m = \cos\psi = \pm 1$

In (2-24a), the current in the inner wire of the cage structure is understood to be 1 ampere. The current in each cage wire and shorting wire is 0.25 amperes, by symmetry. Using the segmentation shown in Figure 2-7(b), the inductance is

$$L = L_{11} + 2L_{12} + \frac{L_{22}}{4} + \frac{L_{23}}{2} + \frac{L_{24}}{4} + \frac{L_{66}}{2} + \frac{L_{68}}{2} + \frac{L_{6,10}}{2} + \frac{L_{6,12}}{2} \tag{2-26}$$

When the dimensions of Figure 2-7(a) are substituted into equations (2-25) and (2-26), the inductance L is found to be 0.01125 μH. At 100 MHz, this yields a reactance of 7.069 ohms.

Summing the contributions to the input impedance of the finite conductivity and the inductance yields a total input impedance of 0.0138 + j7.08 ohms for the simplified theory.

The input impedance that was computed using the moment method is given in Figure 2-8. The figure shows impedance values corresponding to three segmentations for each of the three versions of the program, first using single-precision complex arithmetic and storage in the FORTRAN code (COMPLEX*8) and second using double precision complex arithmetic and storage in the FORTRAN code (COMPLEX*16). It can be seen

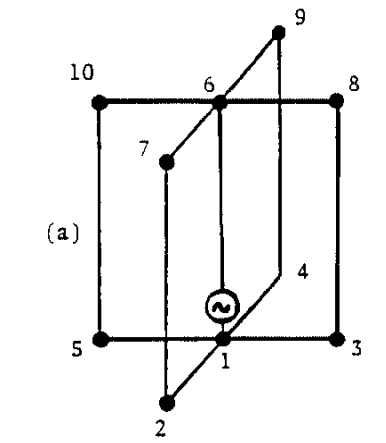

	Impedance (Ω)			
	R	UPC	UBC	Precision
(a)	0.0536 + j19.25	0.0167 + j7.18	0.00711 + j7.10	Single
	0.0139 + j19.25	0.0139 + j7.18	0.0139 + j7.10	Double

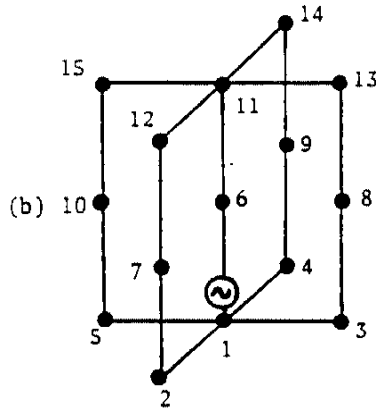

(b)	0.0943 + j14.04	0.0171 + j7.38	0.0327 + j7.10	Single
	0.0140 + j14.04	0.0139 + j7.38	0.0139 + j7.10	Double

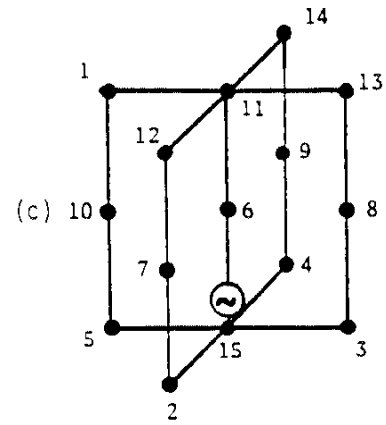

(c)	0.186 + j0.544	0.0110 + j7.39	0.0353 + j7.10	Single
	0.0293 + j0.537	0.0139 + j7.38	0.0139 + j7.10	Double

Fig. 2-8 Impedance of short-circuited cage transmission line for frequency of 100 MHz, conductivity of 57 MS/m, and dimensions given in Figure 2-7 computed by R, UPC and UBC moment methods. Dots denote segment endpoints. The impedance obtained from simplified analysis is 0.0138 + j7.08 ohms.

that in all cases, going from single-precision to double-precision affects the reactance values by only 1% in the worst case. However, the resistance values are affected by more than 20% in the best case: hence double precision is necessary for determining resistance. In the comparison of the impedances obtained from the double-precision versions of the program with the impedance obtained from simplified theory, the bridge-current version is superior. It gave the best agreement with the simplified theory, and it was not sensitive to changes in wire segmentation. In each of the three cases shown, it yielded an impedance of 0.0139 + j7.10 ohms compared with 0.0138 + j7.08 ohms from simplified theory. In terms of reactance, the point-charge version gave poorer agreement with the simplified theory and was more sensitive to changes in wire segmentation than was the bridge current version. In terms of resistance, however, the point-charge version gave the same result as the bridge-current version. The original program gave poor agreement with the simplified theory, and was sensitive to changes in segmentation, in terms of both the number of segments and the point numbering system.

2.5.6. Log-Periodic Dipole Antenna

A log-periodic dipole antenna (LDPA) analysis has been done by Vainberg and Balmain [2] using Richmond's original program. They computed asymmetry resonances produced on LPDAs in which the symmetry was destroyed by an extension of one of the monopoles on the antennas. One surprising result was that, in the case of a perfectly symmetric antenna, the program still predicted asymmetry resonances, four of them in the case studied. For a symmetric antenna, the currents on the two feeder wires should be equal and opposite everywhere. Hence, to either side of the antenna, the far **E** field polarized parallel to the feeder wires should be zero. A measure of the "computer gen-

erated asymmetry" therefore is the side radiation, relative to the radiation on the antenna boresight. Vainberg and Balmain found that, with the original program, the side radiation exhibited peaks at four frequencies, with maxima 50 dB below the boresight radiation. They noted that a different segmentation using only one segment per monopole instead of two segments produced a side radiation of 110 dB below the boresight radiation. Thus, the side radiation was quite sensitive to segmentation. In the present work, the above analysis using two segments per monopole was repeated using the bridge-current version. The predicted side radiation versus frequency was plotted, and four rather ill-defined peaks were identified, the highest levels of these peaks being at least 110 dB below the boresight radiation, in contrast to the original program which yielded only 50 dB.

2.6. CONCLUSIONS

Two alternative new versions of Richmond's original program have been presented, namely the point-charge version and the bridge-current version. Compared with the original program and the point-charge version, the bridge-current version has been shown to be the least sensitive to both the model segmentation scheme and the point numbering scheme. It is also in the best agreement with magnetostatic theory for the small rectangular wire loop and the short coaxial-cage transmission line, and as well in the best agreement with transmission line theory for the two-wire quarter-wave stub. Both the rectangular loop and the stub are relevant to the analysis of a log-periodic dipole antenna because they involve close-spaced parallel wires with a short-circuiting wire, similar to the feeder wires of the antenna and their terminations.

The bridge-current version applied to log-periodic antennas suppresses the unwanted "computer-generated asymmetry" to the point where true asymmetry resonances caused by a perturbation in the antenna geometry can be analyzed with confidence. It is expected that this version should be particularly useful in the analysis of other antennas that incorporate parallel feed wires or stubs that are modelled explicitly.

3. A MULTIRADIUS RECIPROCAL IMPLEMENTATION OF THE THIN-WIRE MOMENT METHOD

3.1. INTRODUCTION

The moment method computer program of J.H. Richmond [1] for the electromagnetic analysis of *uniradius* thin-wire structures can display asymmetric artifacts when used to analyze certain symmetric structures, a problem that was corrected by the "bridge-current" formulation, as discussed in the previous chapter. In the present chapter, the bridge-current formulation is extended to allow solution of the *multiradius* problem. A different, approximate multiradius formulation based in part on transmission line theory is included for comparison.

3.2. DESCRIPTION OF MOMENT METHOD VERSIONS

3.2.1. Uniradius Bridge-Current Version

The uniradius bridge-current version forms the starting point for both the multiradius transmission-line and multiradius bridge-current formulations. It is described in detail in the previous chapter, and is described here briefly because it is necessary in order to explain the multiradius bridge-current version.

The wire structure to be modelled consists of straight wire segments, usually shorter than a quarter wavelength, and all of the same radius. Conceptually, a current expansion function is a tubular dipolar current spanning the surface of two adjoining wire segments that are not necessarily collinear. The current on each segment is axially directed, sinusoidally distributed, continuous at the segment junction, and zero at the other end of each segment. The total current at the junction is unity. Each expansion function has a

corresponding indentical tubular testing function, in a coincident location. The mutual impedance between a tubular expansion dipole and a tubular testing dipole is composed of four tubular-monopole-to-tubular-monopole mutual impedances.

The mutual impedance between a tubular expansion monopole and a tubular testing monopole is approximated by the mutual impedance between two filamentary monopoles that are placed on their respective segment axes unless the axes intersect or coincide. If the axes coincide, the expansion monopole is offset by a wire radius in a direction orthogonal to the coincident axes. If the two axes intersect, the expansion monopole is offset by a wire radius in a direction orthogonal to the plane containing both axes. Whenever a filamentary expansion dipole is broken at its vertex, because of these prescribed offsets between its two monopoles and some testing monopole, the break is bridged by a straight, uniformly distributed "bridge current". With this geometry, the bridge current is orthogonal to the testing monopole. Because of this orthogonality, and because of its uniform current distribution, the bridge current does not contribute to the following symmetric integral form for the mutual impedance Z_{ab} between a filamentary testing monopole a and a bridged filamentary expansion dipole b (2-10) :

$$Z_{ab} = j\omega \int\int \left[\frac{\mu}{4\pi} \mathbf{J}_a(\mathbf{r}) \cdot \mathbf{J}_b(\mathbf{r}') + \frac{1}{4\pi\varepsilon} \rho_a(\mathbf{r})\, \rho_b(\mathbf{r}') \right] \frac{e^{-\gamma R}}{R}\, dV'\, dV \qquad \text{(3-1a)}$$

where

$$R = |\mathbf{r} - \mathbf{r}'| \quad , \qquad \text{(3-1b)}$$

and $\mathbf{J}$ and ρ are volume current and charge densities (unit terminal currents have been assumed). Thus the symmetric mutual impedance integral requires explicit computation of only the monopole-to-monopole mutual impedances which involve the monopole currents and the distributed charges. There are no point charges at the segment ends

because current continuity is ensured due to the presence of the bridge current.

3.2.2. Multiradius Bridge-Current Version

Just as with the uniradius bridge-current version, the multiradius bridge-current version approximates the mutual impedance between tubular expansion and testing monopoles by using the mutual impedance between approximately equivalent filamentary expansion and testing monopoles. However, the amount of offset, if required, is modified to become the greater of the two segment radii. This offset is identical to the uniradius offset in the limiting case where the two segments are of equal radius. In addition, this offset scheme is valid in the limiting case where the radius of one segment is arbitrarily small and both axes are coincident (i.e. the segments are collinear). In this case the equivalence of mutual impedance between the pair of tubular monopoles and the pair of filamentary monopoles is exact because of symmetry. Examples showing the offsets involved in a dipole self impedance and a dipole-to-dipole mutual impedance are given in Figure 3-1.

Filamentary monopole-to-monopole mutual impedances are computed using (3-1a) without point charges. As with the uniradius version, a bridge current does not contribute to (3-1a) because of its orthogonality and uniform distribution.

With the above offsets and bridge currents, the mutual impedance between two filamentary monopoles does not depend on which one is the expansion monopole and which one is the testing monopole. The same must therefore be true of filamentary dipoles. Thus, the dipole mutual impedance matrix is symmetrical. This is a necessary and sufficient condition for reciprocity to hold exactly between sources in the presence of any thin-wire structure that is modelled by the moment method.

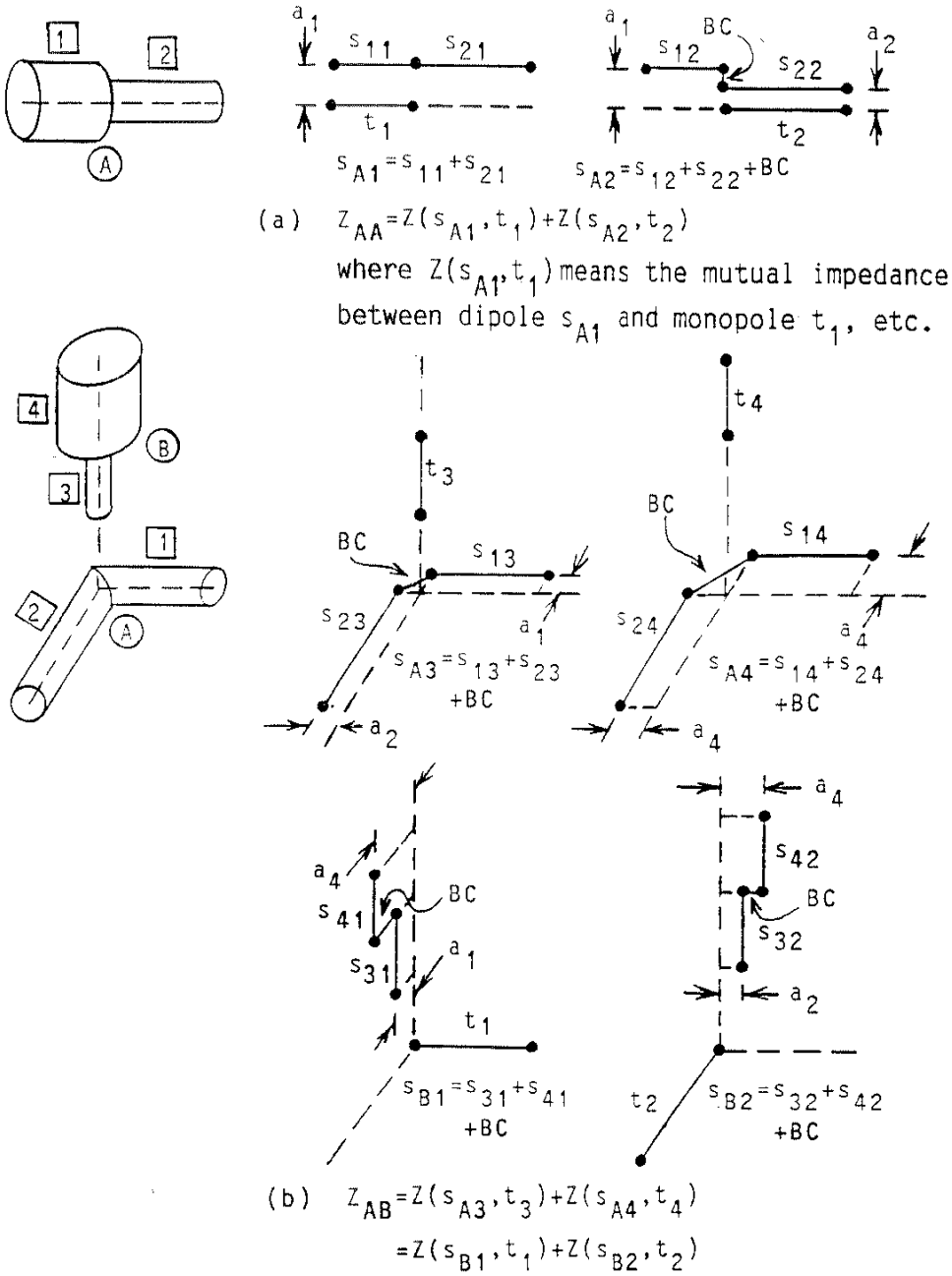

Fig. 3-1 Filamentary currents used to compute approximately (a) the self impedance Z_{AA}, and (b) the mutual impedance Z_{AB}, of tubular dipoles. Circled letters and boxed numbers indicate tubular dipoles and monopoles. Dots denote endpoints of filamentary monopoles. t_j is a filamentary monopole having a longitudinal current distribution equal to tubular monopole j, and lying on the axis of j. s_{ij} is a filamentary monopole having longitudinal current distribution equal to tubular monopole i, but displaced from the axis of i in a manner that depends on tubular monopoles i and j. BC denotes bridge current, and a_i is the radius of monopole i. The point charge contribution of any monopole t_j is neglected.

3.2.3. Transmission-Line Multiradius Version

The transmission-line multiradius formulation was developed as an alternative method to account for the effect of differing segment radii at a wire junction. It is included here because it helps to validate the multiradius bridge-current formulation, which uses a completely different approach to the multiradius problem.

Consider a multiradius thin-wire structure, which has each wire segment covered by a conducting sleeve, where all sleeves are of a single radius that is equal to the largest segment radius or not much larger. Furthermore adjacent sleeves do not touch. If the sleeves are not connected and if all the segment lengths, and hence sleeve lengths, are electrically short, the sleeves will have little effect on the structure's induced currents and scattered fields. Consider sleeves that can be connected by enforcing currents to flow between them. The sleeved segments are depicted schematically in Figure 3-2, where three adjacent segments are shown, along with pairs of terminals. Electric current sources flow across pairs of terminals where arrows point in the reference directions for current flow and increasing voltage. The self impedance Z_{aa} and mutual impedance Z_{ab} are typical terms that must be computed in order to fill the mutual impedance matrix in the multiradius problem. Although the sleeve-to-sleeve currents and sleeve-to-wire currents are all set to zero when computing Z_{aa} and Z_{ab}, they are not all set to zero when computing the *components* of Z_{aa} and Z_{ab} as explained below.

The self impedance Z_{aa} can be decomposed as follows:

$$Z_{aa} = \frac{V_a}{I_a}\Big|_{I_{k\neq a}=0} = \frac{V_{a1}+V_{a2}+V_{a3}}{I_a}\Big|_{I_{k\neq a}=0} = \sum_{i=1}^{3} Z_{ai,a} \qquad \text{(3-2a)}$$

where $Z_{ai,a}$ is the mutual impedance between ports ai and a. By reciprocity,

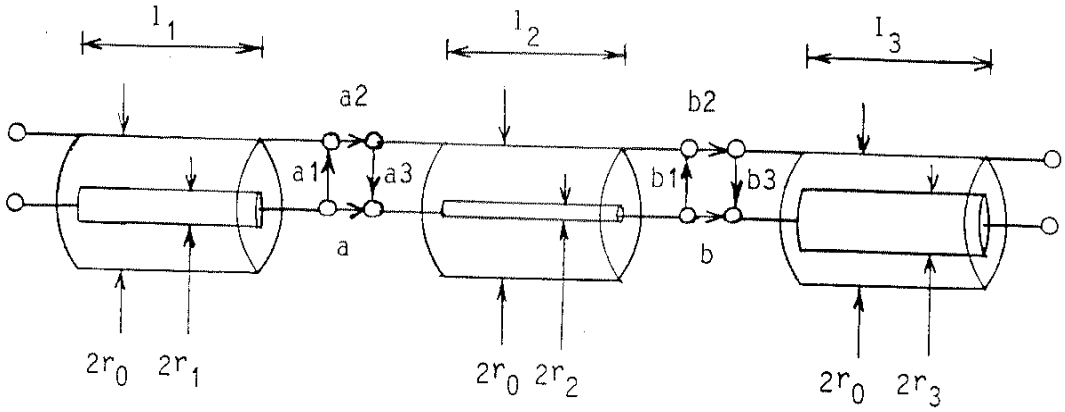

Fig. 3-2 Schematic of 3 adjacent sleeved wire segments with pairs of terminals used in the derivation of the transmission line multiradius modification. Arrows across the pairs of terminals denote reference directions for current flow and increasing potential.

$$\sum_{i=1}^{3} Z_{ai,a} = \sum_{i=1}^{3} Z_{a,ai} \tag{3-2b}$$

The mutual impedance $Z_{a,ai}$ can also be decomposed, as follows:

$$Z_{a,ai} = \frac{V_a}{I_{ai}} \Big|_{I_{k\neq ai}=0} = \frac{V_{a1}+V_{a2}+V_{a3}}{I_{ai}} \Big|_{I_{k\neq ai}=0} = \sum_{j=1}^{3} Z_{aj,ai} \tag{3-2c}$$

$$\sum_{j=1}^{3} Z_{aj,ai} = \sum_{j=1}^{3} Z_{ai,aj} \tag{3-2d}$$

$$Z_{aa} = \sum_{i=1}^{3}\sum_{j=1}^{3} Z_{ai,aj} \tag{3-2e}$$

Regarding the sleeved wire segments as coaxial transmission lines, one deduces that $Z_{a1,\,aj}$ for $j\neq 1$, and $Z_{ai,\,a3}$ for $i\neq 3$ are zero, leaving

$$Z_{aa} = Z_{a2,\,a2} + Z_{a1,\,a1} + Z_{a3,\,a3} \tag{3-2f}$$

$$= Z_{a2,a2} + \frac{\eta}{2\pi} \ln \frac{r_0}{r_1} \coth \gamma l_1 + \frac{\eta}{2\pi} \ln \frac{r_0}{r_2} \coth \gamma l_2 \tag{3-2g}$$

In the above equation, $Z_{a2,\,a2}$ can be computed with the uniradius moment method, and the last two terms have been derived from transmission line theory, where η and γ are the intrinsic impedance and propagation constant of the medium.

The mutual impedance Z_{ab} can be decomposed similarly as follows:

$$Z_{ab} = \frac{V_a}{I_b} \Big|_{I_{k\neq b}=0} = \frac{V_{a1}+V_{a2}+V_{a3}}{I_b} \Big|_{I_{k\neq b}=0} = \sum_{i=1}^{3} Z_{ai,b} \tag{3-3a}$$

$$\sum_{i=1}^{3} Z_{ai,b} = \sum_{i=1}^{3} Z_{b,ai} \tag{3-3b}$$

$$Z_{b,ai} = \frac{V_b}{I_{ai}} \Big|_{I_{k\neq ai}=0} = \frac{V_{b1}+V_{b2}+V_{b3}}{I_{ai}} \Big|_{I_{k\neq ai}=0} = \sum_{j=1}^{3} Z_{bj,ai} \tag{3-3c}$$

$$\sum_{j=1}^{3} Z_{bj,ai} = \sum_{j=1}^{3} Z_{ai,bj} \tag{3-3d}$$

$$Z_{ab} = \sum_{i=1}^{3} \sum_{j=1}^{3} Z_{ai,bj} \tag{3-3e}$$

Again, regarding the sleeved wire segments as coaxial transmission lines, one deduces that $Z_{a1,bj}$, $Z_{ai,b3}$, $Z_{a3,bj}$ for $j \neq 1$, and $Z_{ai,b1}$ for $i \neq 3$ are zero, leaving

$$Z_{ab} = Z_{a2,b2} + Z_{a3,b1} \tag{3-3f}$$

$$= Z_{a2,b2} - \frac{\eta}{2\pi} \ln \frac{r_0}{r_2} \operatorname{csch} \gamma l_2 \tag{3-3g}$$

In the above, $Z_{a2,b2}$ can be computed with the uniradius moment method, and the last term has been derived from transmission line theory.

The above results are also valid if the radius of the sleeve, r_0, is smaller than the smallest segment radius, or alternatively is some intermediate radius.

An interesting result of (3-2g) is that in the case of a half-wave dipole antenna in free space, analyzed in the above manner using two quarter-wave segments, the self impedance does not depend on the wire radius. This agrees with the plotted results in Jordan and Balmain [8] derived from the induced-emf method and the sinusoidal current assumption.

3.3. VALIDATION OF MULTIRADIUS MOMENT METHOD VERSIONS

Computations using the bridge-current multiradius version have been compared (1) with the transmission-line multiradius version, and with simplified theory for the electrically small rectangular loop and coaxial cage transmission line; (2) with transmission-line theory for a resonant two-wire stub and a resonant coaxial cable stub; (3) with measurements for the folded monopole antenna, the sleeve monopole antenna, and the log-periodic dipole antenna; and (4) with a combination of the bridge-current uniradius version and transmission-line theory for the bazooka-balun-fed dipole antenna.

The moment-method programs were written in Fortran 77, and used double precision for all complex numbers and functions. The double precision was previously found to be necessary to obtain accurate input resistances for electrically small structures.

3.3.1. Rectangular Loop

The rectangular loop geometry is shown in Figure 3-3. Actually, three geometries are involved in which the only difference is in wire radius. In geometry 1, all four wires are equal in radius. In geometry 2, the wire radius ratio at each of the four junctions is 10:1, while in geometry 3, the wire radius ratio is 2:1 at two junctions, and 10:1 at the other two junctions as detailed in the caption. For perfectly conducting wire and a frequency of 100 MHz, the input impedance corresponding to each of the three geometries was computed using a simplified theory, and using the moment method versions. The simplified theory included the radiation resistance and the magnetostatic inductance. An assumption of uniform current distribution was used because the loop perimeter is only 0.075 wavelengths. The radiation resistance was computed by means of numerical integration of the radiated power flowing through a spherical surface in the far-field region. A resistance of 19.53 μΩ was obtained. In the inductance computation, the mutual inductance L_{ab} between wires a and b was computed with the following formula which is the magnetostatic version of (3-1a) :

$$L_{ab} = \frac{\mu}{4\pi} \int\int \mathbf{J}_a(\mathbf{r}) \cdot \mathbf{J}_b(\mathbf{r}') \frac{1}{R} \, dV \, dV' \tag{3-4}$$

where the volume current distributions $\mathbf{J}_a$ and $\mathbf{J}_b$ have no divergence, hence have no associated charge, and unit total current is assumed on each wire. A filamentary current approximation was made in which the mutual inductance between two parallel wires is

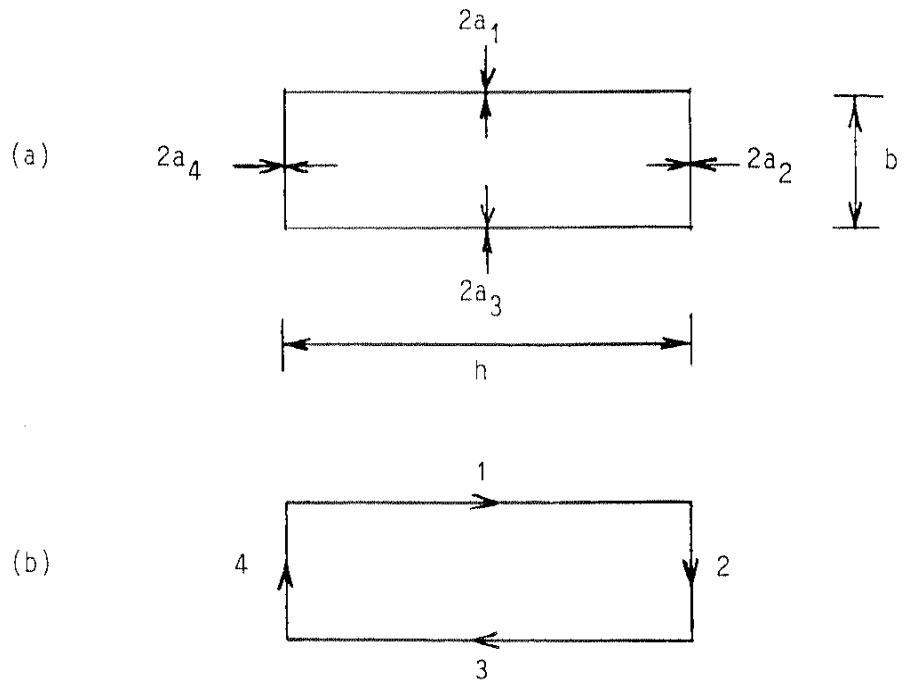

Fig. 3-3 Rectangular Loop

(a) Geometry in which b = 7.5 mm and h = 30 mm. For geometry 1, $a_1 = a_2 = a_3 = a_4 = 1.25$ mm. For geometry 2, $a_1 = a_3 = 1.25$ mm and $a_2 = a_4 = 0.125$mm. For geometry 3, $a_1 = 1.25$ mm, $a_2 = a_4 = 0.125$ mm and $a_3 = 0.250$ mm.

(b) Segmentation for simplified analysis. Segment numbers are shown along with arrows to define reference directions for current flow.

approximated by the mutual inductance between two uniform current filaments on the wire axes. The self inductance of a wire is approximated by the mutual inductance between two uniform current filaments spaced a wire radius apart. The mutual inductance between orthogonal wires is ignored, because orthogonal currents have no mutual inductance according to (3-4). For geometries 1, 2 and 3, the computed inductances are 0.02374, 0.03022, and 0.03968 μH. Geometry 1 is a uniradius structure, and its inductance of 0.02374 μH compares well with the value of 0.02377 μH that was obtained from a U.S. National Bureau of Standards formula (2-18).

Three moment method versions were used. The MBCTL1 version uses the transmission-line multiradius theory along with the uniradius bridge-current theory, with an associated reference radius (i.e. auxiliary sleeve radius) equal to the minimum wire segment radius. The MBCTL2 version uses the same theory, but with a reference radius equal to the maximum wire segment radius. Ideally, these two versions should yield the same answer, but because the transmission-line multiradius theory is approximate, the answers differ slightly (by up to around 3%). Finally, the MBC version uses the multiradius bridge-current theory. Figure 3-4 shows the computed results for various segmentations and generator positions. It appears that all moment method versions are insensitive to changes in segmentation, provided that the generator is not moved significantly, as seen in Figures 3-4 (a), (b) and (e), or (c), (d), (f), and (g). Note that all three moment method versions give the same result for any particular segmentation in geometry 1 because this has a uniform wire radius. In the other two geometries, the three versions give results that differ only slightly from each other, with the MBC result and the simplified result each falling between the MBCTL1 and MBCTL2 results. The MBC result agrees well with the simplified theory (a maximum difference of 1.4% in resistance

Segmentation	Theory	Geometry 1 R(μΩ)	Geometry 1 X(Ω)	Geometry 2 R(μΩ)	Geometry 2 X(Ω)	Geometry 3 R(μΩ)	Geometry 3 X(Ω)
na	simplified	19.53	14.92	19.53	18.99	19.53	24.93
a)	MBCTL1	19.37	14.95	19.65	18.75	19.63	24.82
	MBCTL2	19.37	14.95	19.37	19.30	19.34	25.37
	MBC	19.37	14.95	19.38	19.03	19.49	24.98
b)	MBCTL1	19.36	14.95	19.65	18.75	19.63	24.82
	MBCTL2	19.36	14.95	19.37	19.30	19.34	25.37
	MBC	19.36	14.95	19.38	19.03	19.49	24.98
c)	MBCTL1	19.40	14.94	19.76	18.75	19.97	24.86
	MBCTL2	19.40	14.94	19.47	19.30	19.67	25.41
	MBC	19.40	14.94	19.48	19.03	19.81	25.01
d)	MBCTL1	19.39	14.95	19.74	18.76	19.91	24.87
	MBCTL2	19.39	14.95	19.44	19.31	19.61	25.41
	MBC	19.39	14.95	19.46	19.04	19.75	25.02
e)	MBCTL1	19.36	14.96	19.65	18.75	19.65	24.84
	MBCTL2	19.36	14.96	19.36	19.30	19.36	25.39
	MBC	19.36	14.96	19.38	19.03	19.51	24.99
f)	MBCTL1	19.38	14.95	19.73	18.76	19.90	24.87
	MBCTL2	19.38	14.95	19.44	19.31	19.62	25.42
	MBC	19.38	14.95	19.45	19.04	19.75	25.02
g)	MBCTL1	19.39	14.95	19.75	18.77	19.92	24.89
	MBCTL2	19.39	14.95	19.44	19.31	19.61	25.42
	MBC	19.39	14.95	19.45	19.04	19.75	25.02

Fig. 3-4 Impedance of rectangular loop for frequency of 100 MHz, infinite conductivity, and three geometries, computed by simplified theory, and by the MBCTL1, MBCTL2 and MBC moment methods. The three geometries differ only in wire radius as detailed in Fig. 3-3. Dots denote segment end-points.

and 0.4% in reactance).

3.3.2. Short-Circuited Coaxial Cage Transmission Line

The coaxial cage geometry is shown in Figure 3-5. As with the rectangular loop, there are three geometries involved that differ only in wire radius, as detailed in the caption. The wire conductivity was 57 MS/m and the frequency was 100 MHz. The input impedance corresponding to each geometry was computed using a simplified theory, which included radiation resistance and inductance, as discussed in the previous section, plus the skin effect due to the finite conductivity. Figure 3-6 shows these results along with the MBCTL1, MBCTL2, and MBC results. The MBCTL1 and MBCTL2 reactances differ by about 3%. It can be seen that repositioning of the generator on the inner conductor of the cage makes less than a 1% change in resistance and reactance for the three moment method versions. As with the rectangular loop, the MBC results (and the simplified-theory reactances) fall between the MBCTL1 and MBCTL2 results. In addition, the MBC result is clearly in the best agreement with the simplified theory, having a maximum difference of 0.3% in reactance. All methods predict essentially the same resistance.

3.3.3. Resonant Two-Wire Quarter-Wave Stub

The input reactance was computed, using transmission-line theory and the moment method, for the two-wire transmission line stub shown in Figure 3-7(a). The line has a width of 7.5 mm and a length of 750 mm which is 0.25 λ at the test frequency of 99.93 MHz. The transmission line is short circuited at one end, and open circuited at the other.

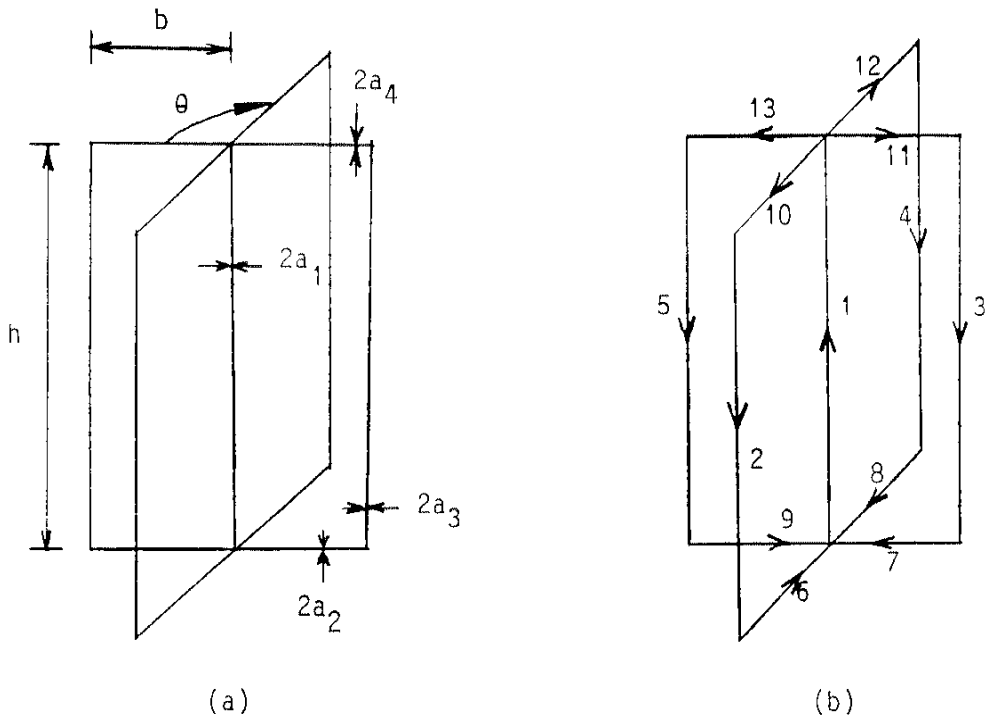

Fig. 3-5 Short-circuited cage transmission line. (a) Geometry in which $b = 7.5$ mm, $h = 30$ mm, and $\theta = 90°$. For geometry 1, $a_1 = a_2 = a_3 = a_4 = 1.25$ mm. For geometry 2, $a_1 = a_3 = 1.25$ mm, and $a_2 = a_4 = 0.125$ mm. For geometry 3, $a_1 = 1.25$ mm, $a_2 = a_4 = 0.125$ mm, and $a_3 = 0.250$ mm. (b) Segmentation for simplified analysis. Segment numbers are shown along with arrows to define the reference directions for current flow.

Segmentation	Theory	Impedance (Ω) at 100 MHz Geometry 1	Geometry 2	Geometry 3
na	simplified	.0138+j7.08	.0251+j8.08	.0352+j9.57
a)	MBCTL1	.0139+j7.10	.0252+j7.92	.0353+j9.45
	MBCTL2	.0139+j7.10	.0252+j8.19	.0353+j9.72
	MBC	.0139+j7.10	.0252+j8.09	.0353+j9.59
b)	MBCTL1	.0139+j7.10	.0252+j7.92	.0353+j9.45
	MBCTL2	.0139+j7.10	.0252+j8.19	.0353+j9.73
	MBC	.0139+j7.10	.0252+j8.09	.0353+j9.59
c)	MBCTL1	.0138+j7.09	.0252+j7.91	.0353+j9.44
	MBCTL2	.0138+j7.09	.0252+j8.19	.0353+j9.71
	MBC	.0138+j7.09	.0252+j8.08	.0353+j9.58
d)	MBCTL1	.0139+j7.10	.0252+j7.92	.0353+j9.45
	MBCTL2	.0139+j7.10	.0252+j8.19	.0353+j9.73
	MBC	.0139+j7.10	.0252+j8.09	.0353+j9.59
e)	MBCTL1	.0138+j7.09	.0252+j7.91	.0353+j9.44
	MBCTL2	.0138+j7.09	.0252+j8.19	.0353+j9.72
	MBC	.0138+j7.09	.0252+j8.09	.0353+j9.58

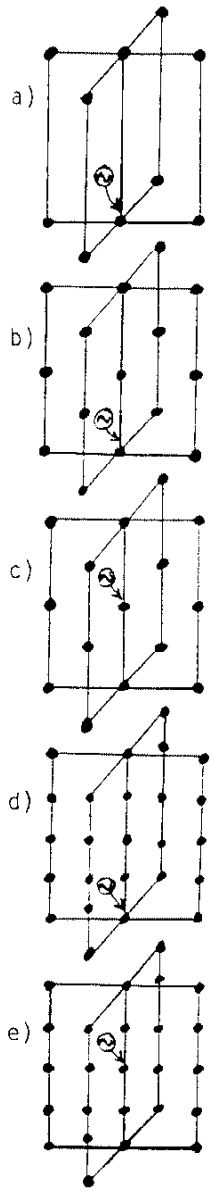

Fig. 3-6 Impedance of short-circuited cage transmission line for frequency of 100 MHz, conductivity of 57 MS/m, and three geometries, computed by simplified theory and by the MBCTL1, and MBCTL2 and MBC moment methods. The three geometries differ only in wire radius as detailed in Fig. 3-5. Dots denote segment endpoints.

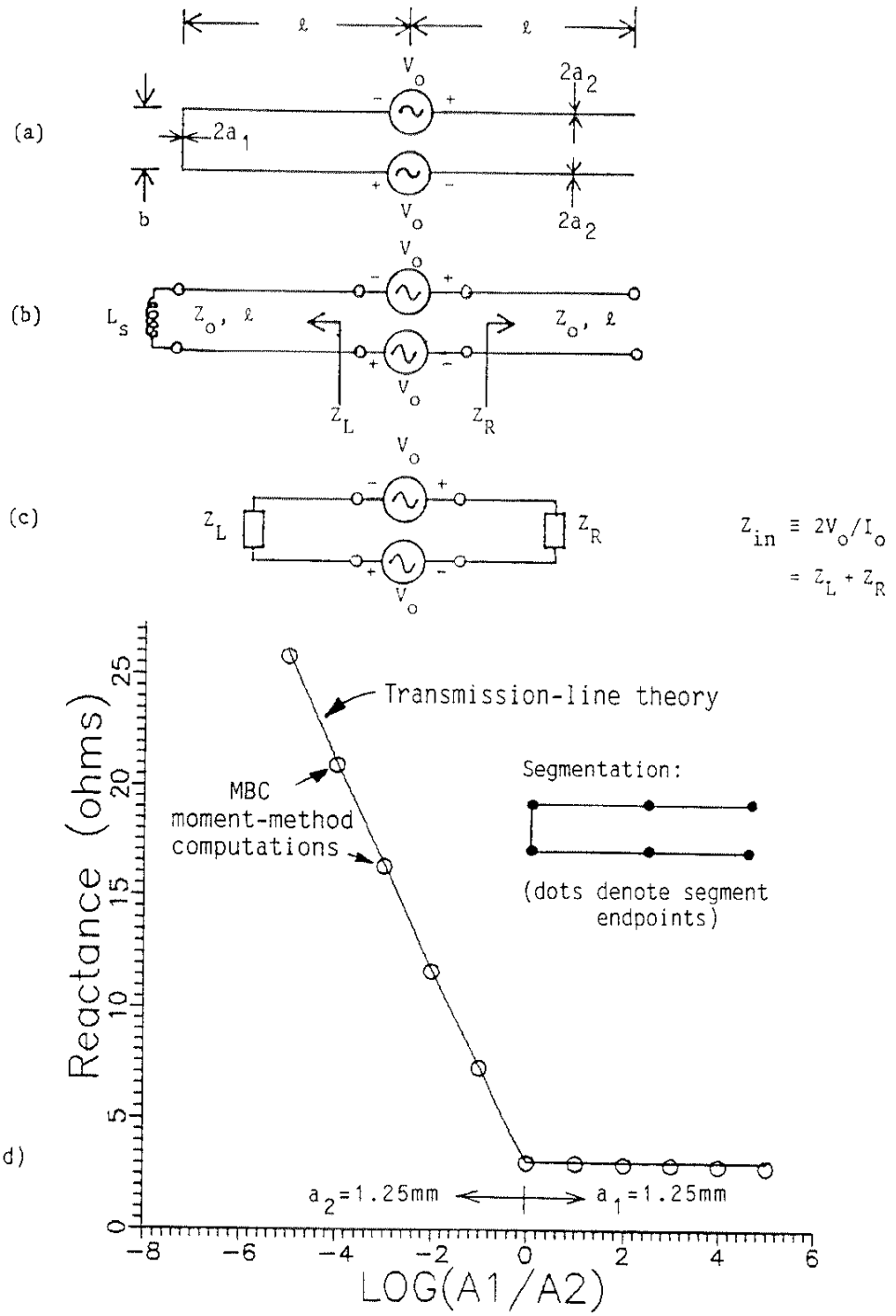

Fig. 3-7 Quarter wave two-wire stub. (a) Feed points and dimensions. (b) Equivalent transmission line circuit. (c) Equivalent lumped element circuit. (d) Reactance for a frequency of 99.93 MHz and infinite conductivity. Transmission line theory (solid line) and MBC moment method computations (circles) are given for the segmentation shown.

Figure 3-7(b) shows the equivalent transmission line circuit. The self inductance, L_S, of the short-circuiting wire is approximately the same as the mutual inductance between two parallel filamentary currents spaced a wire radius apart.

The radius of the shorting wire is a_1, and the radius of the wire forming the transmission line is a_2. The ratio of a_1 / a_2 was varied between 10^{-5} and 10^5 such that the greater of a_1 and a_2 is 1.25 mm. The input reactance, as defined in Figure 3-7(c), was computed with transmission-line theory and with the MBC moment method. The results are plotted in Figure 3-7(d). They show that good agreement was obtained despite the large segment radius ratios of up to 10^5, and the large segment length ratio of 50. The maximum difference is only 0.2 Ω. This is small compared to the characteristic impedance of the transmission line, which varies between 212 Ω and 1044 Ω.

3.3.4. Folded Monopole Antenna

MBC moment method computations of admittance versus frequency for two folded monopole antennas were compared with measurements by German and Brooks [9]. The first resonance of both antennas occurs within the observed frequency range. In one of the antennas, all wires were equal in radius, while in the other antenna, the wires differed in radius by a factor of two. The geometry for the latter case is shown in Figure 3-8. Also shown in the Figure is a convergence test of the MBC moment method. The conductance and susceptance have nearly converged with only three segments on each of the two vertical wires. Only one segment on the short horizontal wire was used throughout. The analysis included an infinite perfectly conducting ground plane. A delta source was used, meaning that the incident E field on the antenna due to the aperture of the coaxial cable was represented as a delta function along the antenna wire just above the ground

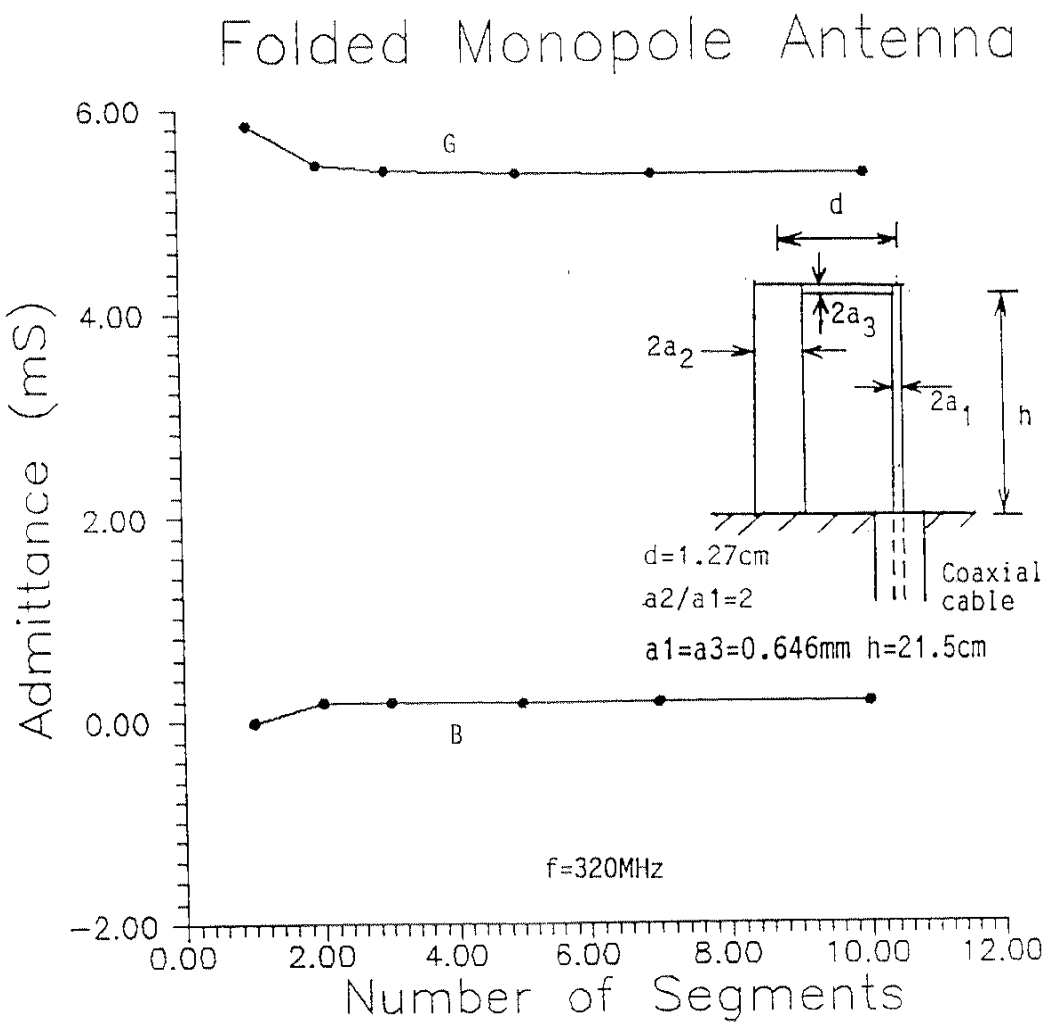

Fig. 3-8 Conductance (G) and susceptance (B) versus number of segments in MBC moment method for folded monopole antenna. The number of segments shown is in each of wires 1 and 2. Dots are computed values, and lines are linear interpolations between the dots. A delta source was used.

plane, and the aperture was filled with conductor to become part of the ground plane.

Figures 3-9 and 3-10 show comparisons between the MBC moment method and measurements for two geometries, labelled A and B. The two geometries differ only slightly in wire spacing (1.20 cm for geometry A versus 1.27 cm for geometry B), but significantly in radius of wire 2 (0.646 mm for geometry A, and twice that for geometry B). It can be seen that the computations are generally in good agreement with the measurements. Moreover, the measured trend in going from geometry A to geometry B is correctly predicted.

3.3.5. Sleeve Monopole Antenna

The sleeve monopole antenna consists of a coaxial cable that extends vertically up above a ground plane for some length, and has the outer conductor and dielectric filling removed over an upper portion of the length, as depicted in Figure 3-11. The surface between the cut end of the outer conductor and the inner conductor is considered to be an aperture. The impedance is defined as the voltage from the outer conductor to the inner conductor at the aperture plane, divided by the current on the inner conductor at the aperture plane.

In the moment method analysis, the aperture is filled in with electric conductor, and an equivalent voltage source is introduced just above the aperture.

MBC moment method computations of the admittance of a sleeve monopole antenna have been compared with measurements by Taylor, presented by King [10], for the geometry shown in Figure 3-11. Initially, poor convergence in the moment method was observed, which was found to be due to the use of a delta source.

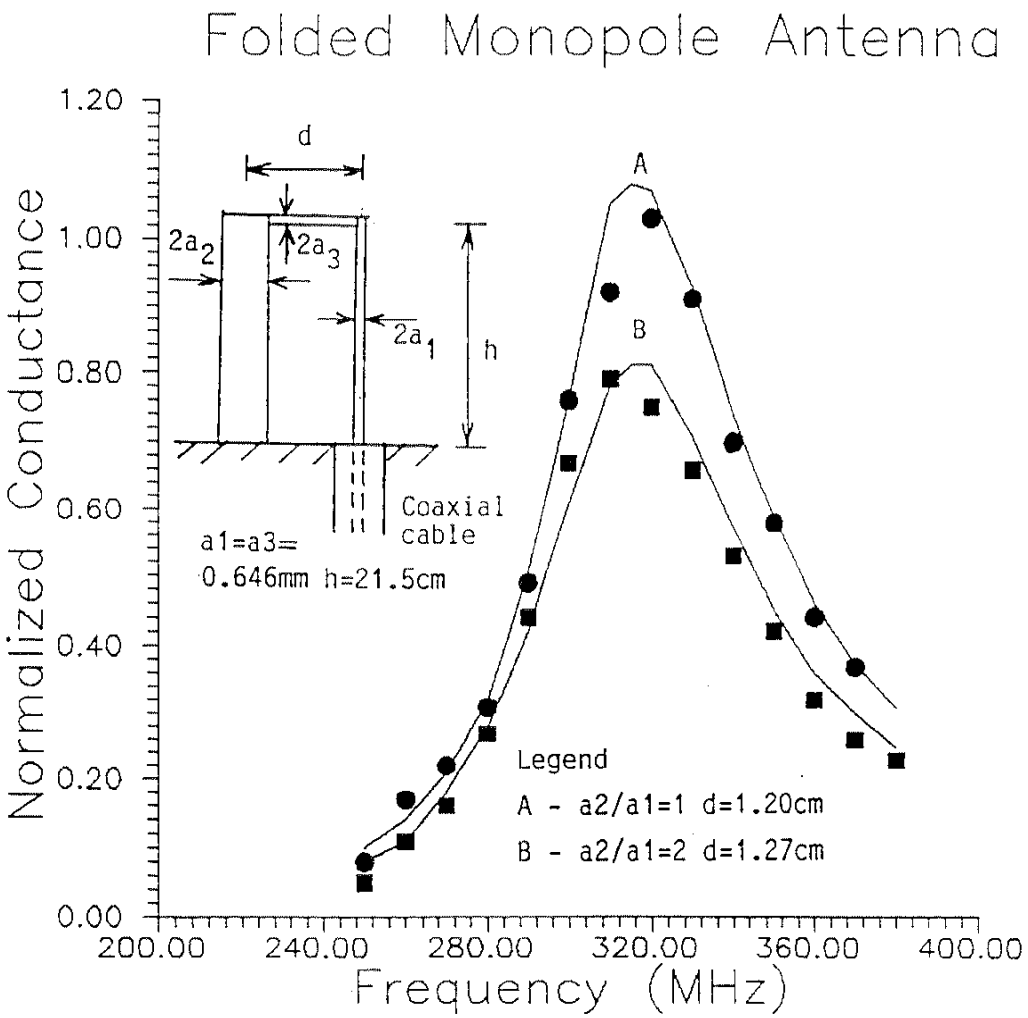

Fig. 3-9 Conductance versus frequency for folded monopole antenna. Dots and boxes denote measured values for the two geometries shown. Lines denote MBC moment method computations using 3 segments on each of wires 1 and 2, and one segment on wire 3. A delta source was used.

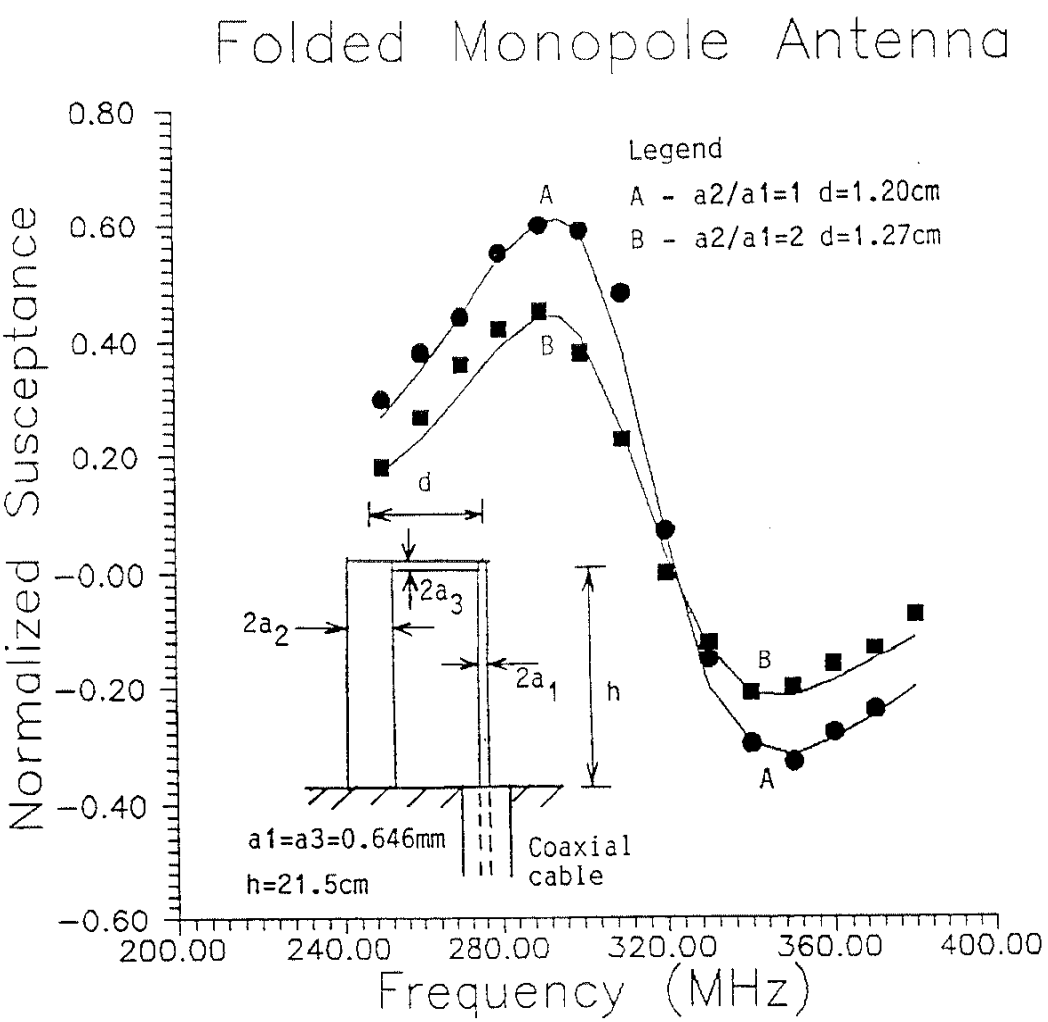

Fig. 3-10 Susceptance versus frequency for folded monopole antenna. Dots and boxes denote measured values for the two geometries shown. Lines denote MBC moment method computations using 3 segments on each of wires 1 and 2, and one segment on wire 3. A delta source was used.

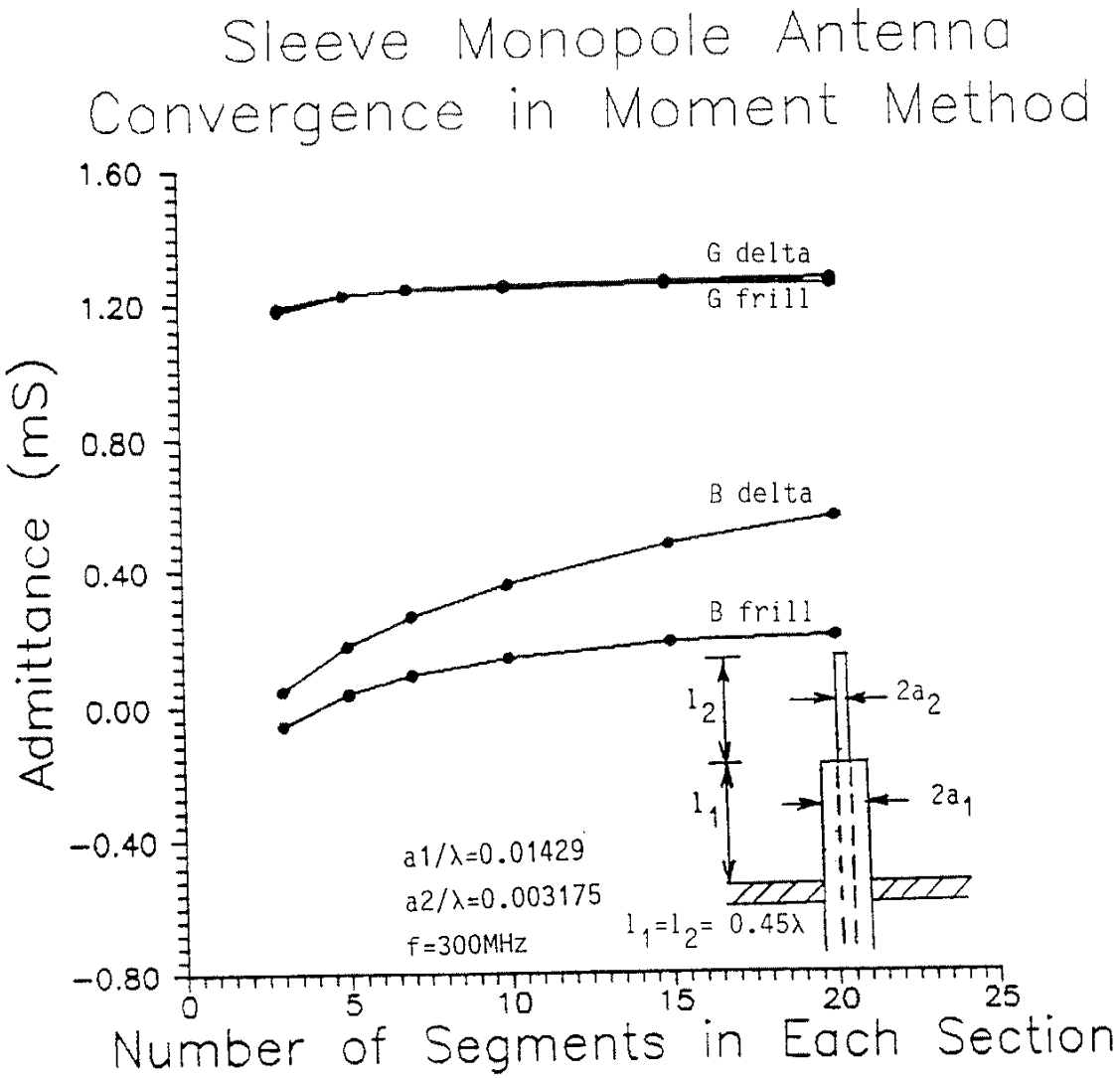

Fig. 3-11 Conductance (G) and susceptance (B) versus number of segments in MBC moment method for sleeve monopole antenna. The number of segments shown is in each of wires 1 and 2. Dots are computed values, and lines are linear interpolations between the dots. One pair of lines is for a frill source, and the other pair is for a delta source.

A delta source is an infinitesimal source that produces a delta function of incident electric field along a testing monopole (whether tubular or filamentary) resulting in a single non-zero term in the moment-method column matrix for voltage. The delta source is a thin-wire approximation to a source consisting of a filamentary magnetic current ring wrapped around a wire, as described in Appendix B. A frill source is a finite-width magnetic current ring which is more realistic, as also described in the Appendix. In order to compute the moment method excitation voltages, each tubular testing monopole is approximated by a filamentary monopole lying on the axis of the tube. This approximation greatly simplifies the computation of the reaction between the source and a testing current.

The use of a frill source resulted in good convergence. The comparison of convergence rates using the frill source and the delta source is shown in the Figure. It appears that the delta source is not acceptable for this problem, probably because of the relatively large electrical radius of the lower section of the antenna (0.014 λ). Good convergence with the frill source was observed when the lengths of the upper and lower sections on the antenna were each 0.15, 0.20, 0.35 and 0.45 wavelengths. The 0.45 wavelength case had the slowest convergence rate, requiring at least 15 segments on each antenna section. This number of segments was selected to be used for all the following computations.

Figures 3-12 and 3-13 compare the computed and measured conductance and susceptance versus the length of each antenna section in wavelengths, shown as case 1. The conductance shows excellent agreement between computations and measurements, with the computed peaks appearing to coincide very well despite their sharpness. The susceptance curves are seen to agree well in shape but the computed values generally need to be

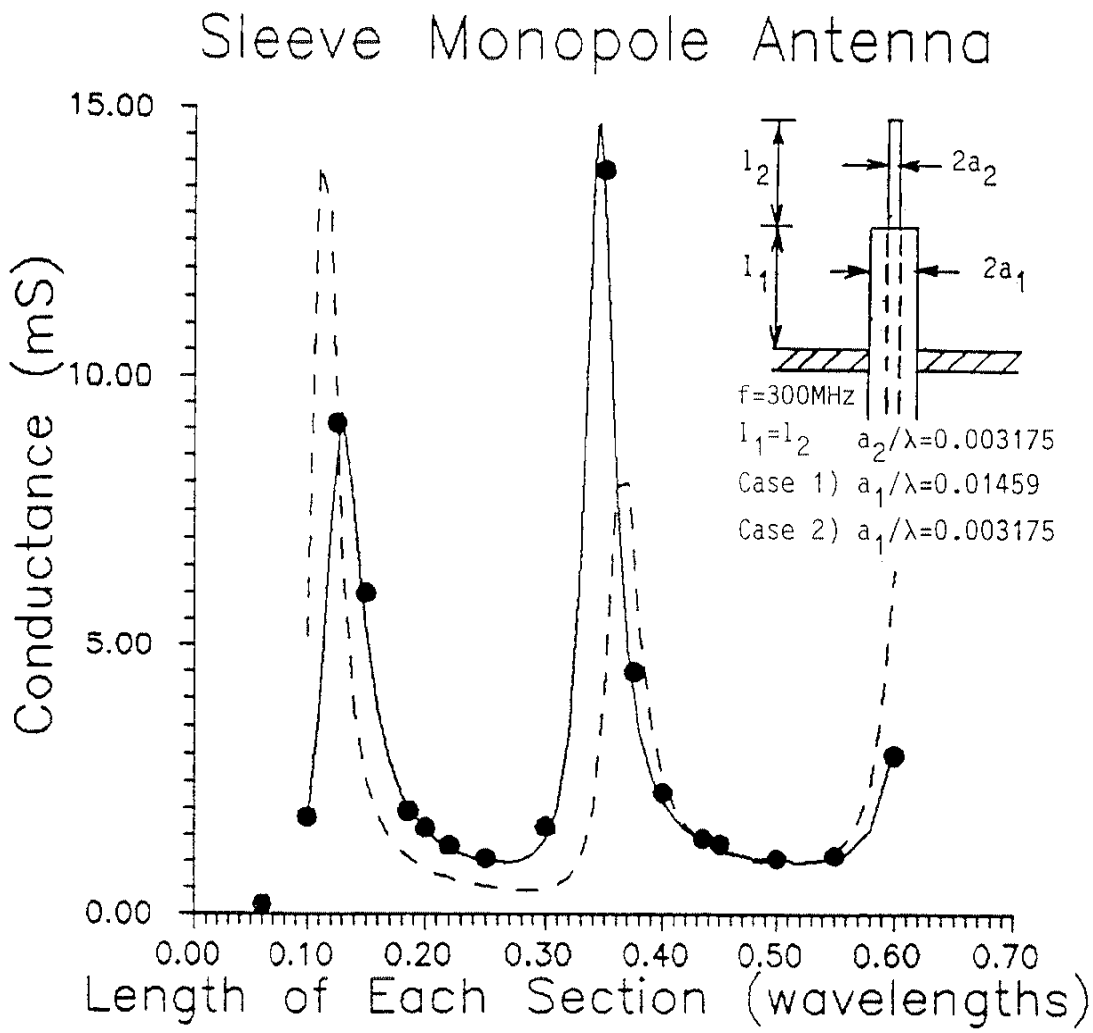

Fig. 3-12 Conductance versus length for sleeve monopole antenna. Dots and solid line denote measurements and MBC moment method computations respectively, for case 1. The dashed line denotes MBC moment method computations for case 2. In both cases, moment method computations include 15 segments in each of wires 1 and 2, and excitation by a frill source whose inner and outer radii are 0.003175λ and 0.01459λ.

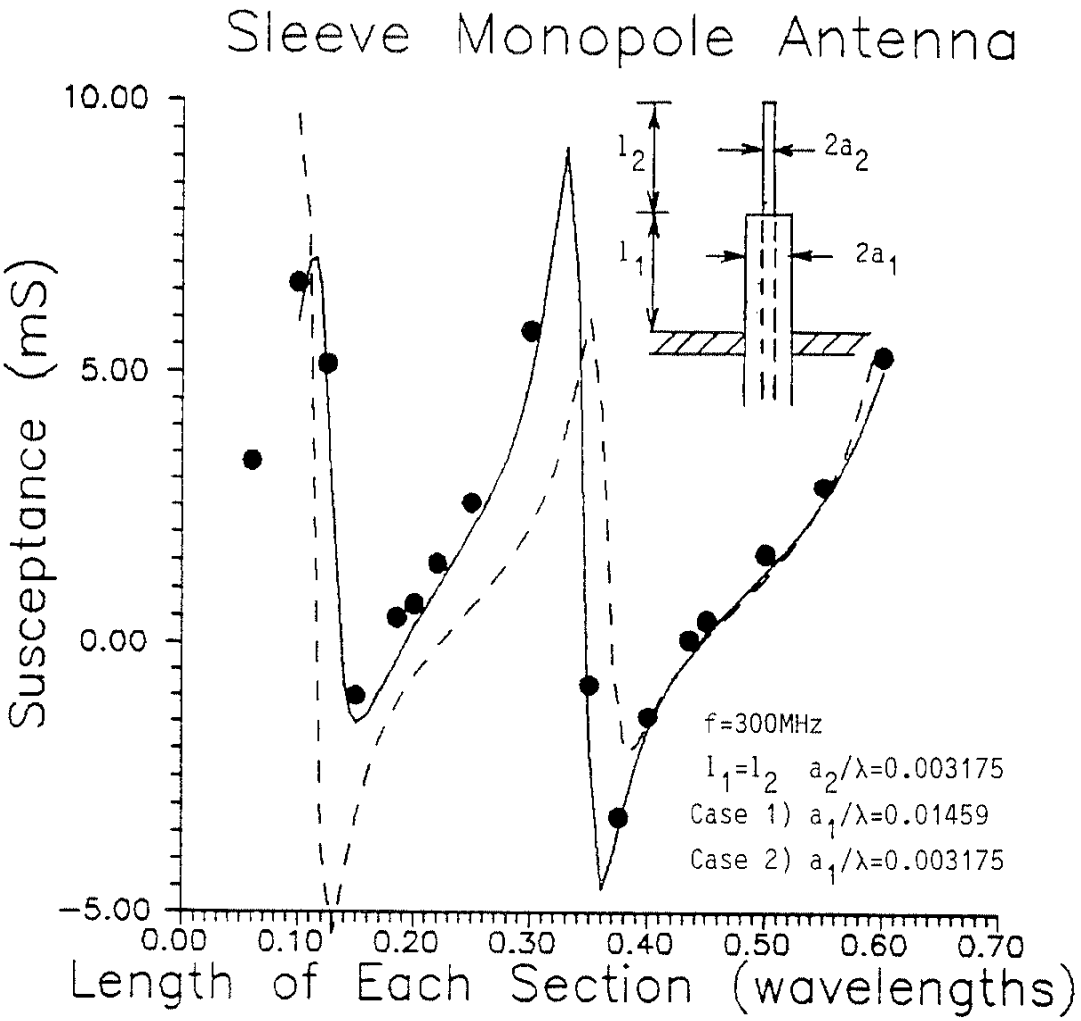

Fig. 3-13 Susceptance versus length for sleeve monopole antenna. Dots and solid line denote measurements and MBC moment method computations respectively, for case 1. The dashed line denotes MBC moment method computations for case 2. In both cases, moment method computations include 15 segments in each of wires 1 and 2, and excitation by a frill source whose inner and outer radii are 0.003175λ and 0.01459λ.

shifted upward by 0.5 mS to agree with the measured ones. This shift is not a large amount, considering that it is equivalent to placing a 0.27 pF capacitor across the aperture.

The dashed lines in the Figures are MBC moment method computations for case 2, which is similar to case 1, except that the radius of the lower half of the monopole is reduced to equal that of the top half. However, the frill source remains unchanged. This case is included to show that the radius change significantly affects the admittance curves.

3.3.6. Log-Periodic Dipole Antenna

Log-periodic dipole antenna (LPDA) analyses and measurements have been done by Vainberg and Balmain [2]. They investigated asymmetry resonances produced on LPDAs in which the symmetry was destroyed by the extension of one of the monopoles on the antennas. Their analysis used a uniradius computer model to approximate the multiradius physical antenna. This was done to enable them to utilize Richmond's (uniradius) thin wire moment-method program [1]. It was noted that the program predicted significant asymmetry resonances even on a symmetric antenna model. This defect in the program was corrected in the previous chapter with the uniradius bridge-current version of the program. In the present section, computations with the uniradius bridge-current version and the multiradius bridge-current version are compared with measurements of the antenna side radiation for an asymmetrical antenna. This side radiation is due to unbalanced current in the two boom wires, and thus is a measure of the strength of the asymmetry resonance phenomenon.

The antenna has 14 monopole elements, labelled 1a, 1b, ... 7a, 7b, as shown in Figure 3-14(a). Also shown in the Figure and caption are all wire dimensions. Monopole 5a is 2.9% longer than monopole 5b, in order to provide a physical asymmetry which will result in side-radiating resonances.

The antenna side radiation versus frequency is shown as the $\theta = 90°$ values in Figure 3-14(b). The solid line shows results of the multiradius program version, while the dashed line shows results of the uniradius program version. The uniradius program version uses a uniradius computer model of the antenna in which the boom diameter and spacing are scaled down by a factor of 2.01 so that the boom conductors are equal in radius to the monopole wires, and the characteristic impedance of the boom conductors remains unchanged. The uniradius results are essentially the same as those obtained by Vainberg and Balmain [2]. They show four well defined resonant peaks that are similar to the measured values, except that they are shifted downward in frequency by approximately 6%, or one third of the spacing between peaks. The multiradius results are seen to be in much better agreement with measured values in terms of resonant frequencies, with a shift in resonant frequency of 0.8% or less. The multiradius program version predicts the level of the four resonant peaks to within 1, 2, 4 and 14 dB as frequency increases. This increasing error probably is due to the fact that, above 660 MHz (between the second and third resonances), the boom conductor radius exceeds the 0.007 λ upper limit originally specified by Richmond for thin-wire theory with a delta source as used in this computation.

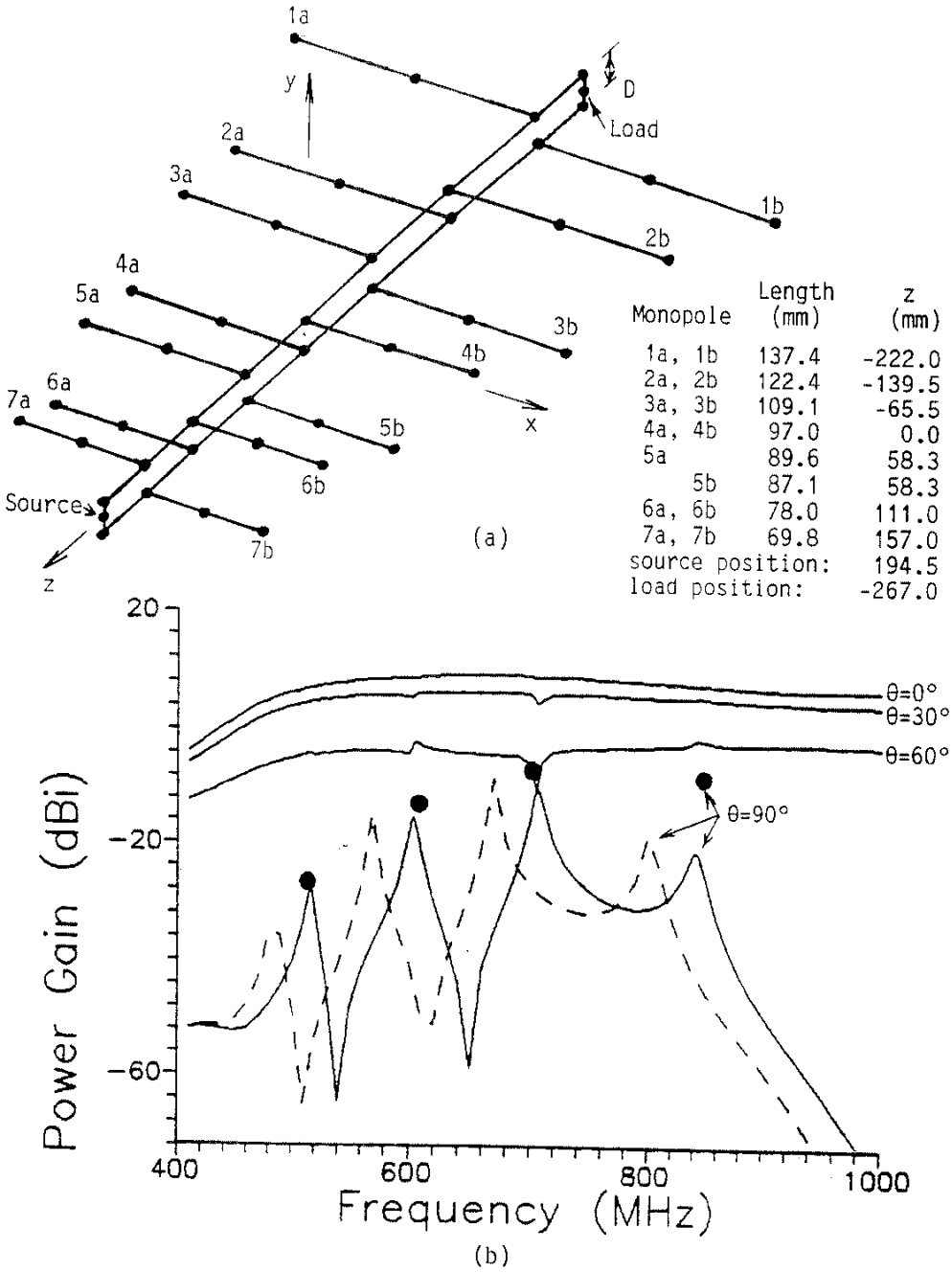

Fig. 3-14 Log periodic dipole antenna. (a) Segmentation and dimensions in computer model. Dots denote segment endpoints. Two cases of geometry are considered: a multiradius case in which all wires are 3.18 mm in diameter except for the z directed boom wires which are 6.40 mm in diameter, with D = 14.6 mm; and a single radius case in which all wires including the boom wires are 3.18 mm in diameter, with D = 7.26 mm. (b) E-plane theta-polarized gain versus frequency for the geometries in (a). Solid dots are measured values, and lines are computed with MBC moment method. Solid lines and solid dots are for the multiradius case. The dashed line is for the single radius case.

3.3.7. Coaxial Cable Stub

Because the filamentary current distributions for testing and expansion currents in the MBC moment method are approximately equivalent to tubular surface distributions of testing and expansion currents, it should be possible to use filamentary currents to analyze structures containing thin concentric cylinders such as coaxial cables. To investigate this, an MBC moment method analysis of a coaxial cable stub was set up as follows for comparison with transmission line theory.

Consider the coaxial cable stub shown in Figure 3-15(a). It has three tubular current-carrying surfaces consisting of the inner and outer surfaces of the outer conductor, and the single surface of the inner conductor. The frequency is 299.8 MHz, and the conductivity is 57 MS/m. Note that, in the moment method analysis, current is allowed to flow radially around the upper lip of the outer conductor, although not much would be expected. However, no radial current is allowed to flow on the bottom surface of the outer conductor, or the top surface of the inner conductor. All radial currents have zero divergence (i.e. no associated charge) because they are represented by uniform bridge currents in the filamentary current approximations.

The transmission-line theory included a series resistance per unit length using the same surface resistance R_s on the tubular metal surface as for a flat metal plate, i.e. the real part of the intrinsic impedance of the metal, which is

$$R_s = \sqrt{\frac{\omega\mu}{2\sigma}} = 4.557 \times 10^{-3}\ \Omega$$

The resistance per unit length of a cylindrical surface is the surface resistance divided by the circumference of the cylinder, which yields 1.012 Ω/m for the inner conductor and

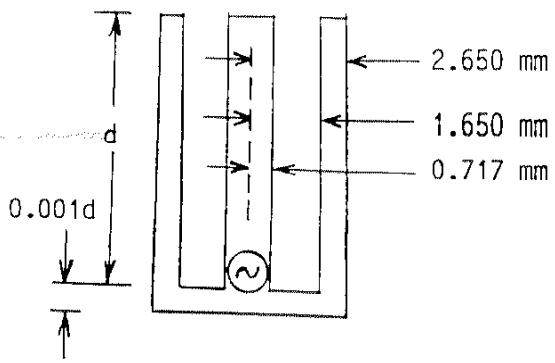

(a)

(b)

Tubular Surface #	First Endpoint	Second Endpoint	Length	Radius (mm)
1	1	2	d	0.717
2	1	3	d	1.650
3	3	4	1.01d	2.650

(c)

Fig. 3-15 Computational model of coaxial cable open-circuited stub. (a) Cross-section showing dimensions. (b) Schematic showing axes of tubular surfaces as solid lines, and endpoints of the axes as dots and numbers. Each number represents a distinct electrical connection or a free end. (c) Specifications of tubular surfaces for program input.

0.440 Ω/m for the inner surface of the outer conductor. The sum of these two values is 1.452 Ω/m which is the total series resistance per unit length of the transmission line. The shunt conductance per unit length is zero. The series inductance and shunt capacitance per unit length of the line are 0.1668 μH/m and 66.71 pF/m. Under lossless conditions, these would yield a characteristic impedance of 50 Ω.

The input resistance and reactance versus transmission line length are shown in Figure 3-16. The MBC moment method results, which used 3 segments per tubular surface, are seen to agree well with the transmission line theory. It was noted that in the MBC results, current flowed radially over the upper lip of the outer conductor. The magnitude of this current was 17% of the generator current when the length was 0.25 λ.

An alternative moment method analysis was done in which the wall thickness of the outer conductor was reduced to zero. Thus, the outer conductor's outer and inner surfaces formed one single surface. This was modelled using only the first two of the three surfaces defined in Figure 3-15(c). The MBC moment method computations using this model agreed as well with transmission-line theory as did the computations with the finite wall thickness.

The above comparisons were repeated for a short-circuited stub, and similarly good agreement was found.

3.3.8. Bazooka Balun Feed for a Dipole Antenna

Consider the dipole antenna fed by a bazooka balun, as shown in Figure 3-17(a). With the dipole half-length of 234.4 mm, the dipole should be nearly resonant at a frequency of 299.8 MHz, at which the wavelength is 1 m. The dipole is fed by a 50 Ω coaxial cable whose length is 250 mm. In a real antenna, the cable would be much longer,

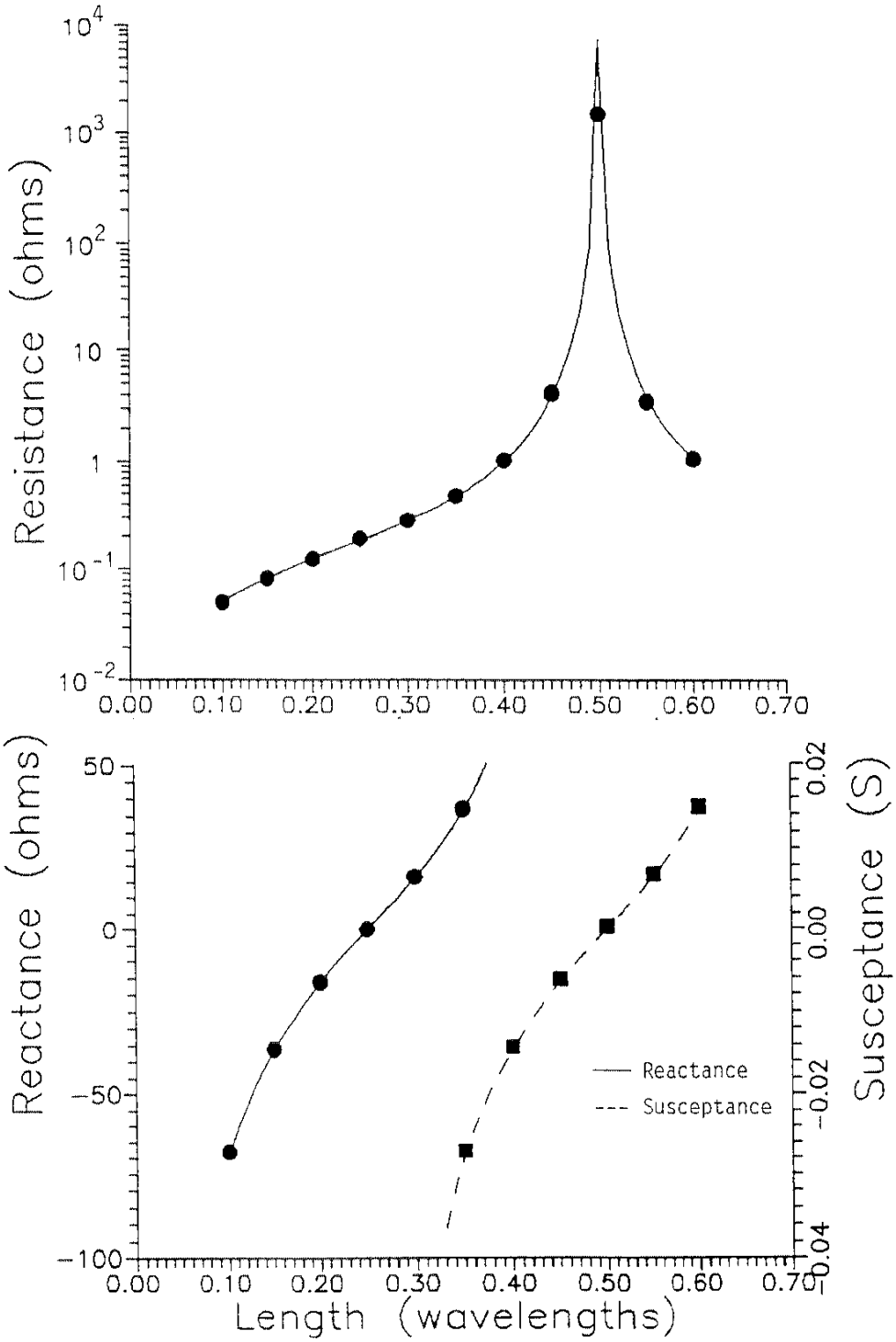

Fig.3-16 Impedance of coaxial cable open-circuited stub shown in Figure 3-15. The frequency is 299.8 MHz and the conductivity is 57μS/m. Lines are derived from transmission-line theory and dots and boxes are derived from the MBC moment method with a delta source and 3 segments per tubular surface.

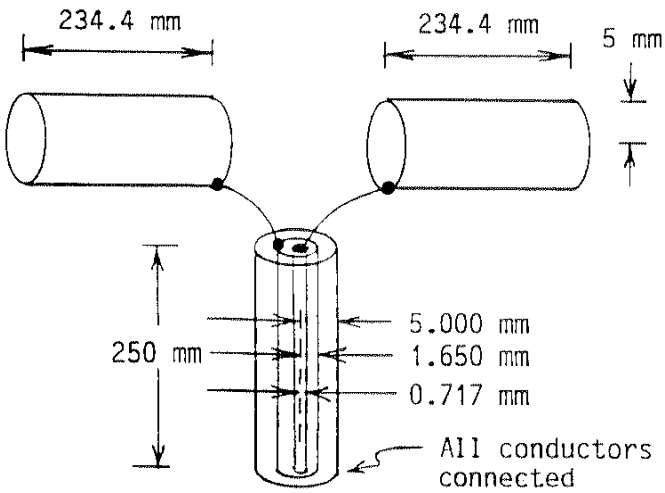

Tubular Surface #	First Endpoint	Second Endpoint	Length (mm)	Radius (mm)
1	1	2	234.4	5.000
2	5	3	234.4	5.000
3	4	1	250.0	0.717
4	4	5	250.0	1.650
5	4	6	250.0	5.000

(c)

Fig. 3-17 Dimensions and connections in bazooka balun-fed dipole antenna. (a) Sketch of possible physical construction. (b) Schematic of moment-method model showing axes of tubular surfaces as solid lines, and endpoints of the axes as dots and numbers. Each number represents a distinct electrical connection or a free end. (c) Specifications of tubular surfaces for program input.

and would connect to some receiving or transmitting equipment. However, in the present example, a short cable was used with a voltage source at the base of the inner conductor, just above the connection between the inner and outer conductors. A conducting sleeve 0.25 λ in length (250 mm) is placed around the cable and shorted at the bottom. This is to prevent current from running down the outside of the cable thereby producing an unbalanced dipole current and cross-polarized radiation.

A moment-method model of this antenna is shown in Figure 3-17(b). All conductors have infinite conductivity, and the wall thickness of both the outer cable conductor and the sleeve is zero, thus allowing them each to be modelled as single surfaces. This approximation was previously found to be valid for the coaxial stub. Note that the modelling of the junction region is approximate. In particular, although the three wires representing the two dipole arms and the sleeve have equal radii, and have a common physical junction, they are not electrically joined. Thus, an "infinitesimal gap" is included in the model. This approximation is similar to the infinitesimal gap approximation associated with a delta voltage source or a delta load.

An MBC moment method analysis with 3 segments per tubular surface yielded an input impedance of 35.0 + j0.0 ohms. The same result was also obtained by computing the input impedance of the dipole alone, without any stub, (71.4 + j0.0 ohms) and transforming this impedance along the 0.25 λ coaxial cable using transmission-line theory. Note that the analysis of the simple dipole involved only a uniradius structure, hence only uniradius theory was required. The computations also yielded maximum copolarized and cross-polarized gains of 1.63 and 3.24×10^{-9} for the balun-fed dipole, and 1.63 and 0 for the simple dipole.

The above was repeated with the sleeve removed. The MBC moment method analysis of this coax-fed dipole yielded copolarized and cross-polarized gains of 0.97 and 0.57, thus demonstrating the expected result that the sleeve is necessary to prevent a significant cross-polarized field. This result was compared with a uniradius theory analysis. The uniradius model was arrived at by moving the voltage generator up along the inner conductor of the coaxial cable until it was just above the open end of the cable. Then the open end was covered with conductor. This yields a uniradius T structure, with a voltage generator on one arm of the T, next to the junction. The uniradius analysis of this T structure yielded the same copolarized and cross-polarized gains that were obtained with the previous multiradius analysis of the coax-fed dipole. In addition, the input impedance of 41.6 - j6.3 ohms for the uniradius T structure, when transformed along the 0.25 λ coaxial cable using transmission line theory, becomes 58.7 + j8.9 ohms, which equals the result obtained using the multiradius analysis of the coax-fed dipole.

3.4. CONCLUSIONS

The multiradius MBC moment method implementation presented herein has been validated in a number of ways. Results computed using this implementation were found to be bracketed by results from two versions of an approximate moment-method formulation using transmission-line concepts to extend uniradius theory to the multiradius case. Comparisons were made both with simplified theories and with experiments. The validation process involved the analysis of the following multiradius thin-wire structures: a small rectangular loop, a small coaxial cage transmission line, a resonant two-wire stub, a folded monopole antenna, a sleeve monopole antenna, a log-periodic dipole antenna (LPDA), a resonant coaxial cable stub, and a bazooka-balun-fed dipole antenna. The

latter two cases demonstrated the multiradius moment-method program's capability to model thin coaxial cables in a way that is both simple and self-consistent; however, the formulation is limited to homogeneous media, so the media inside and outside the cable must be the same.

The structures mentioned above include combinations of simple inductors, transmission lines, and antennas both with and without wires that have free ends. They also include both broadband structures and narrowband structures.

Some of the wire modelling quantities that the program has handled successfully in the above examples include a maximum wire radius ratio of 10^5 for joined wires, a maximum segment length ratio of 50 for joined segments, a maximum of 3 coaxial tubular conducting surfaces, a minimum segment length of 0.0025 λ, and a minimum segment length-to-radius ratio of 6 (1 in the case of the sleeve monopole). These quantities are not necessarily limits of validity. They are merely examples that were studied. They show that the program allows the accurate and stable modelling of a very wide range of wire structures.

The successful multiradius analysis of the asymmetric LPDA, including explicit modelling of the boom, has not previously been done, to the best of the author's knowledge. The presented MBC moment method results agree well with measurements of the asymmetry-resonance frequencies and side-radiation levels. To obtain this agreement, it was necessary to use the physical boom dimensions for the wire radius and spacing, rather than the scaled-down dimensions that were previously used to permit a uniradius analysis. This establishes that the boom plays a crucially important part in the asymmetry resonance phenomenon. Moreover, this example shows that the LPDA pro-

vides a good general test case for a computational technique because it contains multiradius multiwire junctions, parallel wires carrying transmission-line modes, wires with free ends, and closed wire loops.

4. ADVANTAGES OF THE BRIDGE-CURRENT MOMENT METHOD OVER OTHER THIN-WIRE MOMENT METHODS

4.1. INTRODUCTION

In this section, some advantages of the multiradius bridge-current (MBC) thin-wire moment method program over other thin-wire moment method programs are given. The intent is not to make an extensive comparison, which would require coverage of a wide range of situations and many computations. Rather, the intent is simply to show that there are important cases in which the MBC moment method has significant advantages over other popular thin-wire moment methods.

The programs with which the MBC program are compared are the NEC [11] and MININEC [12]. Although the NEC and MININEC have similar names, their expansion and testing functions are quite different. Version number 1 of NEC was used.

Although NEC also handles patches, the discussion here will be restricted to wires. NEC uses expansion functions that consist of sine, cosine and constant current distributions over each segment. Besides enforcing Kirchhoff's current law at segment junctions, NEC also enforces a charge condition such that the electric scalar potential is approximately constant across segment junctions, a procedure which has been found to produce smooth near fields. For testing, delta functions are used (i.e. point matching). As mentioned in the NEC documentation, the program has been used successfully to model a wide range of antennas on complex environments such as ships.

MININEC was developed with emphasis on compatibility with microcomputers. For this reason, the expansion functions are less sophisticated than NEC. For expansion functions, MININEC uses pulses of constant current. Each junction of N segments is

the vertex of $N-1$ pulses. A pulse spans from the midpoint of a segment, to the segment junction, to the midpoint of an adjoining segment. Pulse testing is used, with the approximation that the field over the pulse equals the field at the pulse vertex. Furthermore, in computing the electric scalar potential of an expansion pulse, the point charge that would appear at the edge of a current pulse, i.e. at the midpoint of a segment, is treated as if it were uniformly distributed over the segment. The MININEC documentation includes examples of successful antenna analyses. This program seems to be one of the more popular thin-wire moment method programs, probably because it is easy to learn how to use, runs on typical microcomputers, and is readily available.

Two examples are selected for analysis. One involves a detuning stub used to minimize reradiation from a grounded tower near a monopole antenna in the AM broadcast band. The other involves a bent two-wire transmission line whose dimensions are typical of what one would find with conducting traces on a printed circuit board.

Because both NEC and MININEC use single precision arithmetic and functions, a single-precision version of MBC is also used.

4.2. TOWER DETUNING STUB

Consider a simplified example of reradiation in the AM broadcast band, as depicted in Figure 4-1(a). At the frequency of 1 MHz, the wavelength is approximately 300 m. Two towers 75 m (0.25 λ) in height and 1 m in diameter are separated by 300 m (1 λ). The tower on the right represents a transmitting antenna. The one on the left represents some parasitic tower, which could be used to support an FM broadcast antenna for example. In order to reduce the amount of reradiation from the parasitic tower, a detuning

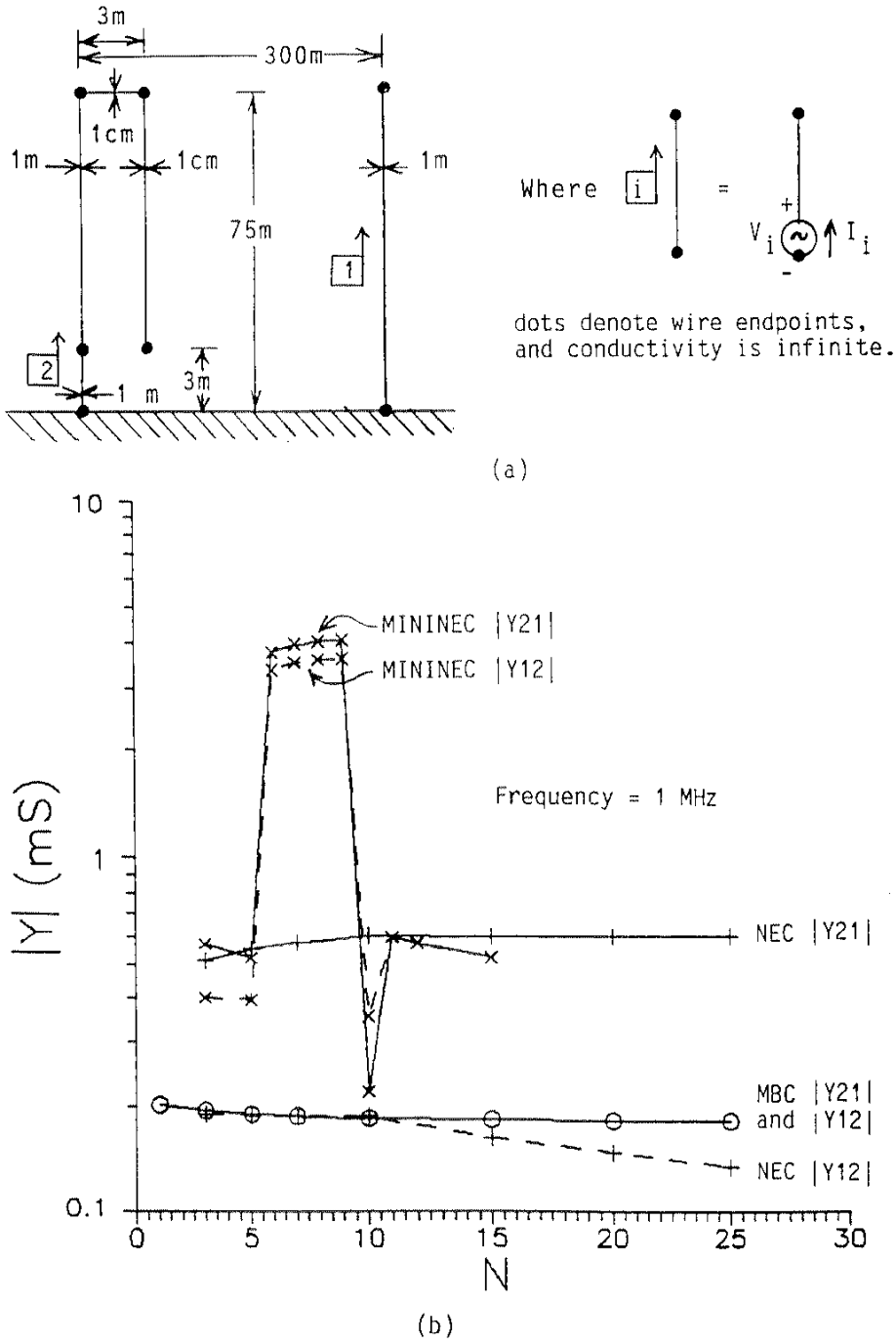

Fig. 4-1 Magnitude of mutual admittance between ports in detuning stub problem. (a) Geometry and port definitions. (b) Computations with MBC, NEC and MININEC moment method programs. The 2 shortest wires have 1 segment each, while the remaining 3 wires have N segments each.

stub has been added, consisting of wire 1 cm in diameter, and spaced 3 m from the tower axis. A common method of testing the effectiveness of the stub is to measure the base current of the parasitic tower (with a small loop antenna). This procedure is simulated on the computer, given a 1 volt source at the base of the transmitting antenna. In other words Y_{21} is computed. As a check on the numerical solution, the reciprocal quantity Y_{12} is also computed. Any difference between these two admittances indicates inaccuracy.

Computations of the mutual admittance magnitudes versus segmentation are shown in Figure 4-1(b). A wide variation in results is seen. The MBC results show good convergence and exact reciprocity. With $N = 7$, the mutual admittance is 0.1877 mS with the stub, compared to 4.554 mS without the stub. This corresponds to a 28 dB reduction in base current due to the stub. The NEC results show significant nonreciprocity even though the Y_{21} appears well converged; however, Y_{12} begins to diverge for $N > 10$. The MININEC results, while showing only slight nonreciprocity, are very erratic as N increases.

In summary, NEC and MININEC display significant errors in this example, while MBC does not.

It should be mentioned that in NEC, the voltages and currents are referred to the segment midpoints, not the segment bases. This is because the "applied E field" source was used. The "current slope discontinuity" source was also tested. As a result of this source, the voltages and currents were referred to the segment bases. At a test segmentation of $N = 7$, the new NEC results were similar to the previous ones, except that the nonreciprocity error was somewhat worse.

4.3. BENT TWO-WIRE TRANSMISSION LINE

This example is a simplified representation of a small portion of a printed circuit board. One must be able to analyse this problem successfully, if one wishes to compute circuit board radiation or susceptibility. Figure 4-2(a) represents two conducting traces on a printed circuit board that run from a pair of pins on one integrated circuit chip to a pair on another. The two wires, which represent traces, can carry a transmission line mode and a radiating mode. Only the transmission line mode is dealt with here: this is done by placing a shorting wire across each end of the transmission line. In the analysis, the four shortest wires, including the two short-circuiting wires, have one segment each, while each of the remaining four wires has a variable number of segments, N. All wires are 0.1 mm in radius and the frequency is 299.8 MHz.

Computations of the mutual susceptance B_{21} versus segmentation are shown in Figure 4-2(b). B_{12} was also computed, but is not shown because there was no significant nonreciprocity in any of the three programs. The MBC computations are seen to be extremely well converged, even when $N = 1$. As a check, B_{21} was also computed with transmission line theory, ignoring the effects of bends in the line and the inductance of the shorting wires. The result was 8.61 mS, which compares well with the value of 8.34 mS obtained by MBC for all N. It can be seen that the NEC results do not converge and are in poor agreement with transmission line theory. MININEC is even worse.

In this example, although NEC and MININEC satisfy reciprocity well, they do not converge, and are inaccurate. On the other hand, MBC shows no sign of error.

It should be mentioned that in MBC and MININEC, the voltages and currents were referred to the segment bases, not their midpoints, for convenience.

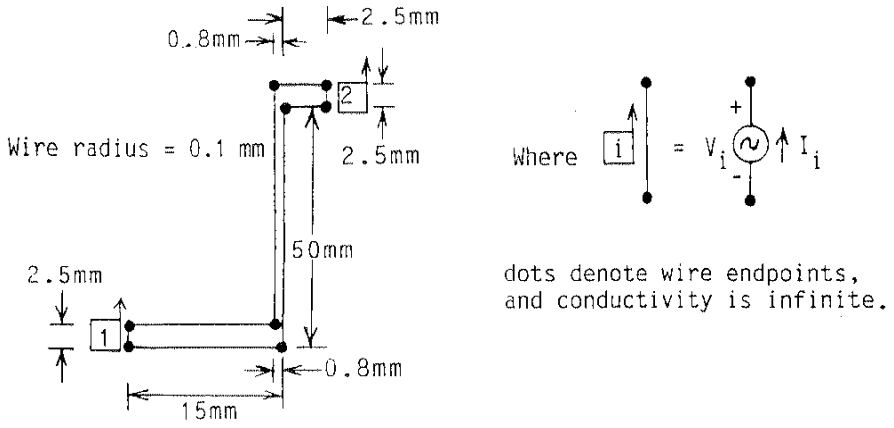

(a)

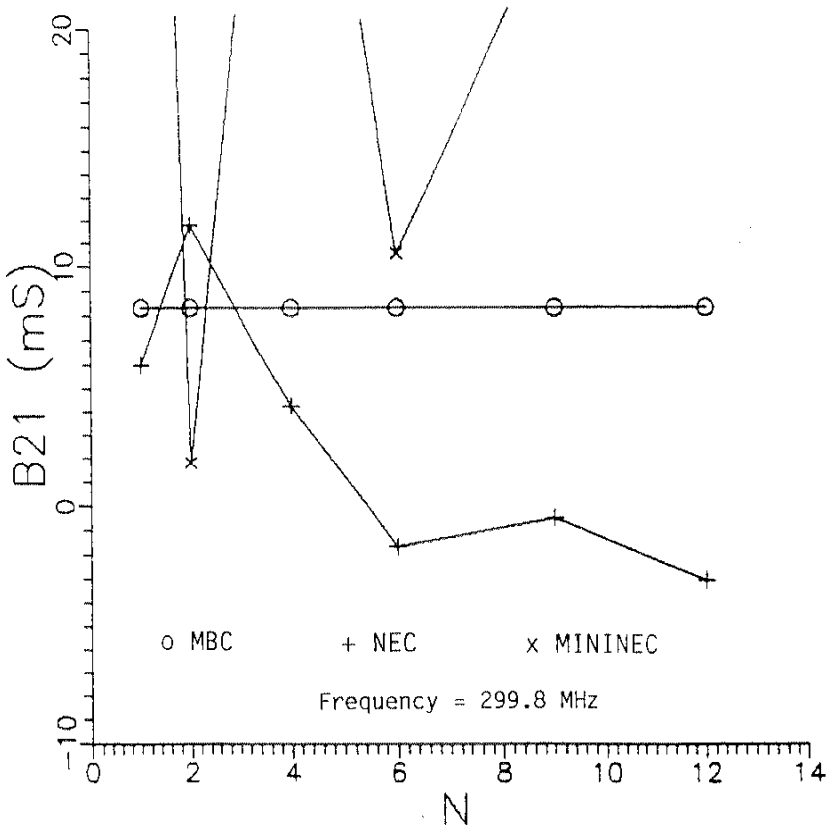

(b)

Fig. 4-2 Mutual susceptance between ports in bent two-wire transmission line. (a) Geometry and port definitions. (b) Computations with the MBC, NEC and MININEC moment method programs. The 4 shortest wires have 1 segment each, while the remaining 4 wires have N segments each. Transmission line theory result is 8.61 mS.

4.4. CONCLUSIONS

The MBC program has some definite advantages over NEC (version #1) and MININEC: in two specific examples described, NEC and MININEC exhibited failure in convergence and non-reciprocity. The MBC program, on the other hand, showed no significant errors.

The examples for which NEC and MININEC had difficulty both involve a transmission line mode with close-spaced wires and a short-circuiting wire. Structures involving this kind of geometry should be analysed cautiously when using NEC or MININEC.

It was also noted that the NEC displayed substantial nonreciprocity when the structure contained wires of greatly differing radii. Thus, one should be cautious when using NEC to analyse a structure containing large differences in wire radii.

5. CONCLUSIONS

The well respected computer program by J.H. Richmond for the moment-method analysis of *uniradius* thin-wire structures has been studied. It has been discovered that this program can generate large errors resulting from its particular method of handling bent wires.

Two formulations that deal with bent wires more carefully have been developed and programmed. The programs, termed the uniradius point-charge (UPC) version and the uniradius bridge-current (UBC) version have eliminated the errors mentioned above, with the UBC version being superior with respect to convergence.

Based upon the success of the UBC version, two formulations to allow the analysis of *multiradius* wire structures were developed and programmed. These programs are termed the multiradius bridge-current transmission-line (MBCTL) version and the multiradius bridge-current (MBC) version. Both versions have been shown to be accurate, with the MBC version having superior accuracy. The MBC version was validated through various comparisons with simplified theory and with measurements on antennas.

Finally, the MBC version was shown to have definite advantages in some areas over two other popular moment method programs called NEC (version #1) and MININEC. This was demonstrated in two example problems, one related to printed circuit analysis, and one related to AM broadcast reradiation. The advantages observed are the exact satisfaction of the reciprocity principle, and the good convergence rate obtained, even under conditions when NEC and MININEC failed to converge.

APPENDIX A

INTEGRATION OF THE INTEGRAL I_{pq}

The integral is defined as

$$I_{pq} = \gamma \frac{1 + mn \cos \psi}{mn} \int_{t_1}^{t_2} \int_{s_1}^{s_2} \frac{e^{\gamma (ms + nt - R)}}{R} \, ds \, dt \tag{A-1}$$

where $p,q = 1$ or $2 \quad m = (-1)^{p-1} \quad n = (-1)^{q-1}$ (A-2)

and $R = \left[s^2 + t^2 - 2st \cos \psi + d^2 \right]^{1/2}$ (A-3)

s integration:

Let $I_1 = \int_{s_1}^{s_2} \frac{e^{\gamma (ms + nt - R)}}{R} \, ds$ (A-4)

and u = - ms - nt + R

Expressing s, ds and R in terms of u yields

$$I_1 = -m \int_{u(s_1, t)}^{u(s_2, t)} \frac{e^{-\gamma u}}{u + c} \, du \tag{A-5}$$

where $c = nt + mt \cos \psi$

Letting $v = \gamma (u + c) = \gamma (-ms + mt \cos \psi + R)$ (A-6)

gives $I_1 = -me^{\gamma t (n + m \cos \psi)} \int_{v(s_1, t)}^{v(s_2, t)} \frac{e^{-v}}{v} \, dv$ (A-7)

t integration:

Let $I_2 = \int_{t_1}^{t_2} I_1 \, dt$ (A-8)

where $I_{pq} = \gamma \dfrac{1 + mn \cos \psi}{mn} I_2$ (A-9)

Let $U = \int_{v(s_1, t)}^{v(s_2, t)} \dfrac{e^{-v}}{v} \, dv$ (A-10)

and $dV = -me^{\gamma t (n + m \cos \psi)} \, dt$. (A-11)

using $dU = \left[\dfrac{e^{-v}}{v} \dfrac{dv}{dt} \right]_{v(s_1, t)}^{v(s_2, t)} dt$ (A-12)

and integrating by parts as in

$$I_2 = \int UdV = [UV] - \int VdU \tag{A-13}$$

yields $I_2 = \dfrac{1}{\gamma (n + m \cos \psi)} [I_1]_{t_1}^{t_2} + \dfrac{m}{\gamma (n + m \cos \psi)} [I_3]_{s_1}^{s_2}$ (A-14)

where $I_3 = \int_{t_1}^{t_2} \dfrac{e^{\gamma (nt + ms - R)}}{mt \cos \psi - ms + R} \left[m \cos \psi + \dfrac{t - s \cos \psi}{R} \right] dt$ (A-15)

Letting u = - nt - ms + R

and expressing t, dt and R in terms of u yields

$$I_3 = \int_{u(s, t_1)}^{u(s, t_2)} e^{-\gamma u} \frac{u^2 + 2u - u_0^2}{(u^2 + u_0^2)(u + c)} \, du \tag{A-16}$$

where $u_0 = d \left[\dfrac{1 + mn \cos \psi}{1 - mn \cos \psi} \right]^{1/2}$ (A-17)

and $c = ms + ns \cos \psi$

expanding the rational polynomial in the integral yields

$$I_3 = \int_{u\,(s,\,t_1)}^{u\,(s,\,t_2)} e^{-\gamma u} \left(-\frac{1}{u+c} + \frac{1}{u+ju_0} + \frac{1}{u-ju_0} \right) du \tag{A-18}$$

Letting

$$w = \gamma\,(u+c) = \gamma\,(-nt + ns\cos\psi + R)\ , \tag{A-19}$$

$$x = \gamma\,(u+ju_0) = \gamma\,(-ms - nt + R + ju_0)\ , \tag{A-20}$$

and

$$y = \gamma\,(u-ju_0) = \gamma\,(-ms - nt + R - ju_0)\ , \tag{A-21}$$

yields

$$I_3 = -e^{\gamma s\,(m\,+\,n\cos\psi)} \int_{w\,(s,\,t_1)}^{w\,(s,\,t_2)} \frac{e^{-w}}{w}\,dw \tag{A-22}$$

$$+ e^{\gamma j u_0} \int_{x\,(s,\,t_1)}^{x\,(s,\,t_2)} \frac{e^{-x}}{x}\,dx + e^{-\gamma j u_0} \int_{y\,(s,\,t_1)}^{y\,(s,\,t_2)} \frac{e^{-y}}{y}\,dy$$

Substituting the expression for I_3 and I_1 into I_2

$$I_{pq} = \left[-e^{\gamma t\,(n+m\cos\psi)} \int_{v\,(s_1,\,t)}^{v\,(s_2,\,t)} \frac{e^{-v}}{v}\,dv \right]_{t_1}^{t_2} \tag{A-23}$$

$$+ \left[-e^{\gamma s\,(m\,+\,n\cos\psi)} \int_{w\,(s,\,t_1)}^{w\,(s,\,t_2)} \frac{e^{-w}}{w}\,dw + e^{\gamma j u_0} \int_{x\,(s,\,t_1)}^{x\,(s,\,t_2)} \frac{e^{-x}}{x}\,dx \right.$$

$$\left. + e^{-\gamma j u_0} \int_{y\,(s,\,t_1)}^{y\,(s,\,t_2)} \frac{e^{-y}}{y}\,dy \right]_{s_1}^{s_2}$$

The integration variables consist of a complex constant multiplied by a real function that is sometimes added to an imaginary constant. The integration path is therefore a straight line on the complex plane. The integrals are of the form

$$W\,(z_1, z_2) = \int_{z_1}^{z_2} \frac{e^{-z}}{z}\,dz \tag{A-24}$$

which is evaluated in the original program.

In the case of parallel segments, we have $\cos\psi = \pm 1$.

Case 1) $\quad 1 + mn\cos\psi = 0$

In this case, $u_0 = 0$ and $v = w = x = y = \gamma(-ms - nt + R)$. Also,

$$\left[\int_{v(s_2,\,t)}^{v(s_1,\,t)} \frac{e^{-z}}{z}\,dz\right]_{t_1}^{t_2} = \left[\int_{v(s,\,t_2)}^{v(s,\,t_1)} \frac{e^{-z}}{z}\,dz\right]_{s_1}^{s_2} \tag{A-25}$$

because the integration path is a straight line that has no singularities.

Hence,

$$I_{pq} = \left[(-1-1+1+1)\int_{v(s,\,t_2)}^{v(s,\,t_1)} \frac{e^{-z}}{z}\,dz\right]_{s_1}^{s_2} = 0 \tag{A-26}$$

Case 2) $\quad 1 - mn\cos\psi = 0$

In this case, $u_0 = \infty$

$$e^{\gamma j u_0}\int_{x(s,\,t_1)}^{x(s,\,t_2)} \frac{e^{-z}}{z}\,dz = \int_{t_1}^{t_2} \frac{e^{\gamma(ms+nt-R)}\,dt}{\gamma(-ms-nt+R+ju_0)} = 0 \tag{A-27}$$

and similarly, the integral involving y vanishes. Thus, we have

$$I_{pq} = -\left[e^{\gamma t 2n}\int_{v(s_1,\,t)}^{v(s_2,\,t)} \frac{e^{-z}}{z}\,dz\right]_{t_1}^{t_2} - \left[e^{\gamma s 2m}\int_{w(s,\,t_1)}^{w(s,\,t_2)} \frac{e^{-z}}{z}\,dz\right]_{s_1}^{s_2} \tag{A-28}$$

where $v\ (s,\ t) = \gamma\,(-ms + nt + R)$ (A-29)

and $w\ (s,\ t) = \gamma\,(-nt + ms + R)$ (A-30)

APPENDIX B

MAGNETIC RING SOURCE AND FRILL SOURCE EXCITATION

This appendix derives the excitation voltage of a filamentary monopole of electric current due to both a filamentary magnetic current ring and a frill of surface magnetic current. Only the case in which the ring or loop axis coincides with the monopole axis is covered here.

The excitation voltage V_j of a monopole j due to a general source of magnetic current $\mathbf{M}_g$ according to Richmond [1, eq.(12)] equals the following reaction between the monopole and the general source (assuming unit terminal currents):

$$V_j = -\int \mathbf{H}_j \cdot \mathbf{M}_g \, dv \tag{B-1a}$$

$$= \int \mathbf{E}_g \cdot \mathbf{J}_j \, dv \tag{B-1b}$$

The second equation can be obtained from the first by applying the reciprocity theorem. For convenience, we will use the first equation.

Let the monopole be a linear electric current $\mathbf{I}_j$ on the z axis, flowing between points z_1 and z_2, and having unit feed-point current.

$$\mathbf{I}_j = \hat{\mathbf{z}} \frac{\sinh \gamma (z - z_l)}{\sinh \gamma (z_j - z_l)} \tag{B-2a}$$

$$= \hat{\mathbf{z}} \frac{1}{2 \sinh \gamma (z_j - z_l)} \sum_{p=1}^{2} m e^{-m\gamma z_l} e^{m\gamma z} \tag{B-2b}$$

where $j = 1$ or 2, $l = 2/j$ $m = (-1)^{p-1}$ and $z_1 \le z \le z_2$.

The magnetic vector potential $\mathbf{A}_j$ is

$$\mathbf{A}_j(\mathbf{r}) = \frac{\mu}{4\pi} \int_{z_1}^{z_2} \mathbf{I}_j(z') \frac{e^{-\gamma R}}{R} dz' \tag{B-3a}$$

$$= - \frac{\hat{\mathbf{z}}\mu}{8\pi \sinh \gamma (z_j - z_l)} \sum_{p=1}^{2} m e^{\gamma m (z - z_l)} \int_{u(z_1)}^{u(z_2)} \frac{e^{-u}}{u} du \tag{B-3b}$$

where $R = [\rho^2 + (z' - z)^2]^{1/2}$ and $u(z') = \gamma [R - m(z' - z)]$.

The magnetic field strength $\mathbf{H}_j$ is

$$\mathbf{H}_j = \frac{1}{\mu} \nabla \times \mathbf{A}_j = - \frac{\hat{\phi}}{\mu} \frac{\partial A_{jz}}{\partial \rho} \tag{B-4a}$$

$$= \frac{\hat{\phi}}{8\pi \sinh \gamma (z_j - z_l)} \sum_{p=1}^{2} e^{-\gamma m z_l} \sum_{q=1}^{2} (-1)^q \frac{\rho}{R_q} \frac{e^{-\gamma (R_q - m z_q)}}{R_q - m(z_q - z)} \tag{B-4b}$$

where $R_q = [\rho^2 + (z - z_q)^2]^{1/2}$.

Equation (B-4b) can be rearranged to the following form, which is similar to that given by Richmond [1, eq.(77)].

$$\mathbf{H}_j = \frac{-\hat{\phi}}{4\pi \rho \sinh \gamma (z_j - z_l)} \sum_{q=1}^{2} (-1)^q e^{-\gamma R_q}$$

$$\cdot \left[\cos \theta_q \sinh \gamma (z_q - z_l) - \cosh \gamma (z_q - z_l) \right] \tag{B-5}$$

where $\cos \theta_q = \frac{z - z_q}{R_q}$.

Now consider a filamentary magnetic current ring of radius a, centred at the origin, whose axis coincides with the z axis. The magnetic current $\mathbf{M}_r$ is ϕ - directed, with a value of $-V_0$ volts, as shown below.

$$\mathbf{M}_r = -V_0\,\hat{\phi} \qquad \text{at} \quad \rho = a\ , \qquad z = 0 \tag{B-6}$$

The resultant excitation voltage on the monopole according to (B-1a)

$$V_j = -\int_0^{2\pi} \mathbf{H}_j \cdot \mathbf{M}_r\, \rho\, d\phi \qquad \text{at} \quad \rho = a\ , \qquad z = 0 \tag{B-7}$$

Inserting (B-5) and (B-6) in the above yields

$$V_j = \frac{-V_0}{2 \sinh \gamma (z_j - z_l)} \sum_{q=1}^{2} (-1)^q\, e^{-\gamma R_q} \cdot \left[\cos\theta_q \sinh \gamma (z_q - z_l) - \cosh \gamma (z_q - z_l)\right] \tag{B-8}$$

It is useful to look at the case when the monopole feed-point is at the origin. Let $z_1 = 0$, $z_2 = d$, and $j = 1$. The result is

$$V_1 = \frac{V_0}{2}\, \frac{e^{-\gamma a} \cosh \gamma d - e^{-\gamma R_2}}{\sinh \gamma d} \tag{B-9}$$

For a dipole of half length d, centred at the origin, the excitation voltage is twice the above. This excitation voltage magnitude is plotted in Figure B-1 for $V_0 = 1$ volt. Note that for small a/λ, the excitation voltage is approximately unity. In this region a delta source approximation, which assigns all V_0 to one dipole mode, seems to be a good approximation to the magnetic current ring. However, for larger a/λ, it is not a good approximation.

Now consider a frill of magnetic surface current, centred at the origin, whose axis coincide with the z axis. The frill has inner radius a and outer radius b. The surface current $\mathbf{M}_f$ has the same distribution as the E field in a coaxial cable, as follows:

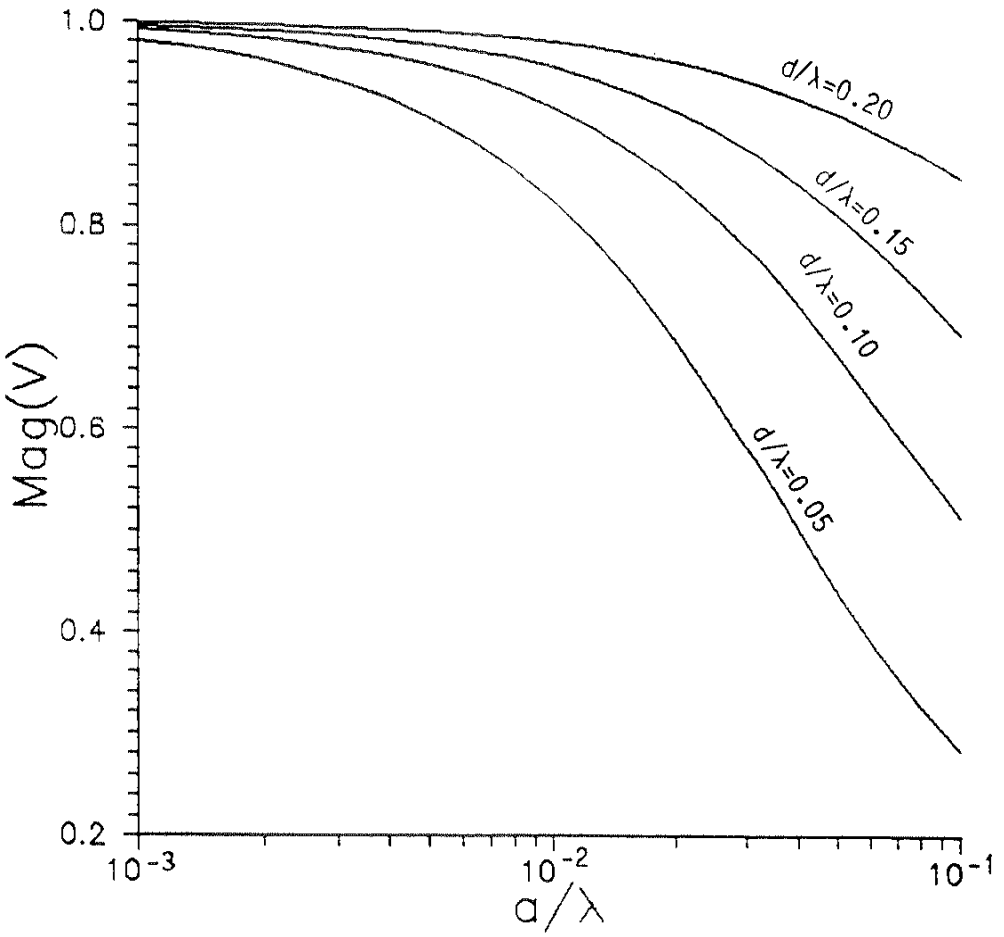

Fig. B-1 Magnitude of excitation voltage on a filamentary dipole of half-length d due to a filamentary magnetic current ring of 1 volt and radius a. The centres and axes of the dipole and ring coincide.

$$\mathbf{M}_f = \frac{-V_0}{\rho \ln b/a}\,\hat{\phi} \text{ at } a \le \rho \le b, \quad z = 0 \tag{B-10}$$

Note that the total ϕ - directed magnetic current is $-V_0$ volts. The **E** field of a frill is given by Butler and Tsai [13]. That would be required if we were using (B-1b). However, we will use (B-1a) instead, as follows:

$$V_j = -\int_a^b \int_0^{2\pi} \mathbf{H}_j \cdot \mathbf{M}_f \, \rho \, d\phi \, d\rho \tag{B-11a}$$

$$= -\frac{2\pi V_0}{\mu \ln (b/a)} \int_a^b \frac{\partial A_{jz}}{\partial \rho}\, d\rho \tag{B-11b}$$

$$= \frac{V_0}{4 \ln (b/a) \sinh \gamma (z_j - z_l)} \sum_{p=1}^{2} m e^{-\gamma m z_l}$$

$$\cdot \sum_{h=1}^{2} (-1)^h \int_{u(z_1, \rho_h)}^{u(z_2, \rho_h)} \frac{e^{-u}}{u}\, du \tag{B-11c}$$

where $u(z', \rho) = \gamma \left[[z'^2 + \rho^2]^{1/2} - mz' \right]$, $\rho_1 = a$ and $\rho_2 = b$.

Note that the integration variable u is a complex constant multiplied by a real function. The integration path is therefore a straight line on the complex plane. The function

$$w_{12}(u_1, u_2) = \int_{u_1}^{u_2} \frac{e^{-u}}{u}\, du \tag{B-12}$$

for a straight line path is evaluated in Richmond's original program [1].

REFERENCES

[1] J.H. Richmond, "Radiation and scattering by thin-wire structures in the complex frequency domain", National Technical Information Service, Springfield, VA 22151, NASA CR-2396, May 1974. Companion computer code: "Computer program for thin wire structures in a homogeneous conducting medium", National Technical Information Service, Springfield, VA 22151, NASA CR-2399, June 1974.

[2] M. Vainberg and K.G. Balmain, "On prediction of the asymmetry resonance phenomenon of log periodic dipole antennas", Can. Elec. Eng. J., vol.6, no.3, 1981, pp. 31-34.

[3] M.M. Silva, K.G. Balmain and E.T. Ford, "Effects of power line reradiation on the patterns of a dual frequency MF antenna", IEEE Trans. Broadcasting, vol. BC-28, no.3, September 1982, pp.94-103.

[4] M. Hilbert, M.A. Tilston and K.G. Balmain, "Resonance phenomena of log-periodic antennas: characteristic-mode analysis", IEEE Trans. Antennas Propagat., accepted for publication.

[5] U.S. National Bureau of Standards, "Radio instruments and measurements", Circular no.74, March 10, 1924, equation 138.

[6] E.C. Jordan and K.G. Balmain, "Electromagnetic waves and radiating systems", Prentice-Hall, 1968, p.562.

[7] p. 598 in reference [6].

[8] p. 548 in reference [6]

[9] J.P. German and F.E. Brooks, Jr., "The effects of the physical parameters on the bandwidth of a folded dipole", IRE Trans. Antennas Propagat., vol. 46, pp. 186-190, April 1958.

[10] R.W.P. King, "The theory of linear antennas", Harvard University Press, Cambridge, Mass., p. 416, 1956.

[11] G.J. Burke and A.J. Poggio, "Numerical electromagnetics code (NEC) - method of moments", National Technical Information Service, Springfield, VA 22151, NOSC TD 116, vol. 1 and 2, July 1977.

[12] J.W. Rockway, J.C. Logan, D.W.S. Tam and S.T. Li, "The MININEC system : microcomputer analysis of wire antennas", Artech House, 1988.

[13] C.M. Butler and L.L. Tsai, "An alternate frill field formulation", IEEE Trans. Antennas Propagat., vol. AP-21, no. 1, pp. 115-116, Jan. 1973.